Petrology and Geochemistry of Mafic-Ultramafic Fragments from the Aguablanca Ni-Cu Ore Breccia, Southwest Spain

R. Piña,† R. Lunar, L. Ortega,

Departamento de Cristalografía y Mineralogía, Facultad de Geología, Universidad Complutense, E-28040 Madrid, Spain

F. Gervilla,

Instituto Andaluz de Ciencias de la Tierra (Universidad de Granada-CSIC) and Departamento de Mineralogía y Petrología, Facultad de Ciencias, E-18071, Granada, Spain

T. Alapieti,

Department of Geoscience, University of Oulu, 90014 Oulu, Finland

and C. Martínez

Río Narcea Recursos, SAU., Mina "Aguablanca," E-41250, Real de la Jara, Sevilla, Spain

Abstract

Aguablanca (southwest Spain) is the first economic Ni-Cu-(PGE) deposit found in southern Europe. Two features make it an unusual example of magmatic sulfide ore: it is related to the development of an Andean-type continental magmatic arc, and it is hosted by a subvertical magmatic breccia. The structural style and the geodynamic context of the deposit contrast with most plutonic Ni-Cu-PGE deposits elsewhere, which occur at specific levels of layered mafic intrusions in rift environments.

The Ni-Cu deposit is hosted by the Aguablanca intrusion, a mafic body composed of gabbronorite and minor quartz-diorite, gabbro, and norite. Sulfides are concentrated in a gabbronorite matrix along a subvertical (dip of 70º–80º N), funnel-like magmatic breccia that contains barren or slightly mineralized ultramafic-mafic cu-mulate fragments. Modal compositions of the fragments reflect a wide variety of rock types, including peri-dotite (hornblende-rich werhlite, dunite, and hornblende-rich harzburgite), pyroxenite (ortho- and clinopyrox-enite), gabbro (gabbro, gabbronorite, and hornblende gabbro), and anorthosite. The primary silicate assemblage includes olivine (Fo_{91}–Fo_{79}), orthopyroxene (Mg no. 0.85–0.73), clinopyroxene (Mg no. 0.93–0.62), plagioclase (An_{99}–An_{38}), amphibole (Mg no. 0.87–0.68) and phlogopite (Mg no. 0.89–0.64). The wide range of rock types and the Fe-enrichment trends in the primary ferromagnesian silicates suggest magmatic differenti-ation processes from the parent melts, with the fragments representing different stages of cumulate formation.

The ore-bearing breccia contains both semimassive and disseminated sulfides in the gabbronorite matrix. Textures vary between meso- and orthocumulate, and the rock-forming magmatic silicates are orthopyroxene (Mg no. 0.83–0.74), clinopyroxene (Mg no. 0.89–0.78), plagioclase (An_{50}-An_{77}), and intercumulus amphibole (Mg no. 0.86–0.70), phlogopite (0.84–0.69) and minor quartz. The gabbronorite in the matrix of the breccia is petrographically and chemically very similar to that of the unmineralized parts of the main Aguablanca intru-sion and exhibits a similar differentiation trend, suggesting that the matrix of the ore-bearing breccia and the unmineralized rocks belong to a same magmatic suite. The local presence of mafic-ultramafic fragments in the barren Aguablanca intrusion supports this suggestion.

The presence of highly Ni depleted olivine, whole-rock Cu/Zr ratios below 1, and the local occurrence of dis-seminations of magmatic sulfides in the peridotite fragments point to sulfide segregation before and/or during the formation of the peridotite cumulates. Mantle-normalized incompatible trace element patterns of the frag-ments along with published sulfur isotope data are consistent with crustal contamination, suggesting that addi-tion of crustal sulfur from pyrite-bearing black slates led to sulfide saturation. These results support a model in which sulfides segregated and settled during the differentiation of an unexposed mafic-ultramafic complex, now sampled as fragments in the breccia, whereas the overlying silicate magma, most probably fed by succes-sive fresh magma injections, underwent fractional crystallization, giving rise to this cumulate sequence. The emplacement of the ore breccia took place at temperatures above the (monosulfide solid solution (mss) solidus but below the olivine and pyroxene solidus, likely owing to the explosive injection of a new pulse of magma into the chamber, which mingled with the sulfide liquid and disrupted the overlying cumulate sequence. As a consequence, fragments reached their current position in the breccia, injected along with the sulfide and the sili-cate melts, which subsequently formed the sulfide-rich gabbronorite.

Introduction

Economic Ni-Cu-PGE deposits associated with mafic-ultramafic rocks are uncommon in Europe. With the exception of the world-class Noril'sk and Pechenga deposits in Russia (Barnes et al., 2001), most occurrences are restricted to Finland—in the Portimo, Penikat, or Koillismaa complexes (Alapieti and Lathinen, 2002), which are currently being evaluated by the Artic Platinum Partnership, and the Vammala,

† Corresponding author: e-mail, rpinagar@geo.ucm.es

Hitura, and Kotalahti deposits (Frietsch et al., 1979). Other known examples include Råna in Norway (Boyd and Mathiesen, 1979) and Ivrea-Verbano in Italy (Garuti et al., 1986). Owing to the scarcity of this type of deposit, the discovery of the economic Aguablanca ore deposit in southwest Spain (lat. 37º57' N, long. 6º11' W) caused an important change in the outlook for the supply of Ni and PGE in southwest Europe. The Ni-Cu sulfide mineralization was discovered in 1993 by Presur-Atlantic Copper S.A. during a regional exploration program which revealed an Ni geochemical anomaly related to a gossan (Lunar et al., 1997; Ortega et al., 2000, 2004). The company carried out detailed work to evaluate the economic potential of the mineralization, with satisfactory results, and the project was subsequently acquired by Rio Narcea Gold Mines Limited in 2001. Reserves of 15.7 million tonnes (Mt), grading 0.66 wt percent Ni, 0.46 wt percent Cu, 0.47 g/t platinum group minerals (PGM), and 0.13 g/t Au were established, and the exploitation of the deposit started at the end of 2004. The discovery of this deposit has promoted an extensive and ambitious exploration program in the region which has led to the identification of more than 100 targets with anomalies similar to those of Aguablanca.

Sulfide ores are hosted by the Aguablanca intrusion within a subvertical magmatic breccia, mainly composed of gabbronorite rocks containing disseminated and semimassive Ni-Cu-Fe sulfides which include numerous barren or slightly mineralized mafic-ultramafic cumulate fragments. Tornos et al. (2001) suggested that fragments came from a hidden mafic-ultramafic complex containing interbedded sulfides which were brecciated by residual silicate melts. More recently, Ortega et al. (2004) examined the mineralogy and geochemistry of the sulfide ore, defining an assemblage of PGM hosted within sulfides composed mainly of (Pd, Pt)-bismuthotellurides. Ortega et al. (2004) proposed a genetic model for the sulfide ores consisting of magmatic crystallization and subsolidus reequilibration of a sulfide liquid, accompanied by the formation of a magmatic PGM assemblage exsolved from the sulfides. Although the evolution of the sulfide ore has been well defined, the origin and nature of the breccias, their genetic relationship to the sulfide-bearing matrix, and their role in the geologic processes involved in the genesis of the ore have not been studied in detail. In this paper we examine the petrography, mineralogy, mineral chemistry, and bulk rock composition of the fragments and the sulfide-bearing matrix of the breccia in order to better understand the mechanisms of crystal fractionation and sulfide-melt segregation in the source chamber of the deposit and the shallow crustal emplacement of the sulfide melt.

Geology of the Aguablanca Intrusion

Geologic background

The Aguablanca intrusion is located in the southern limb of the Olivenza-Monesterio antiform, a west-northwest–east-southeast–trending longitudinal hercynian structure situated in the southern boundary of the Ossa-Morena zone. This zone is one of the five parts of the Iberian Massif (Quesada, 1991, and references therein) (Fig. 1), the westernmost belt

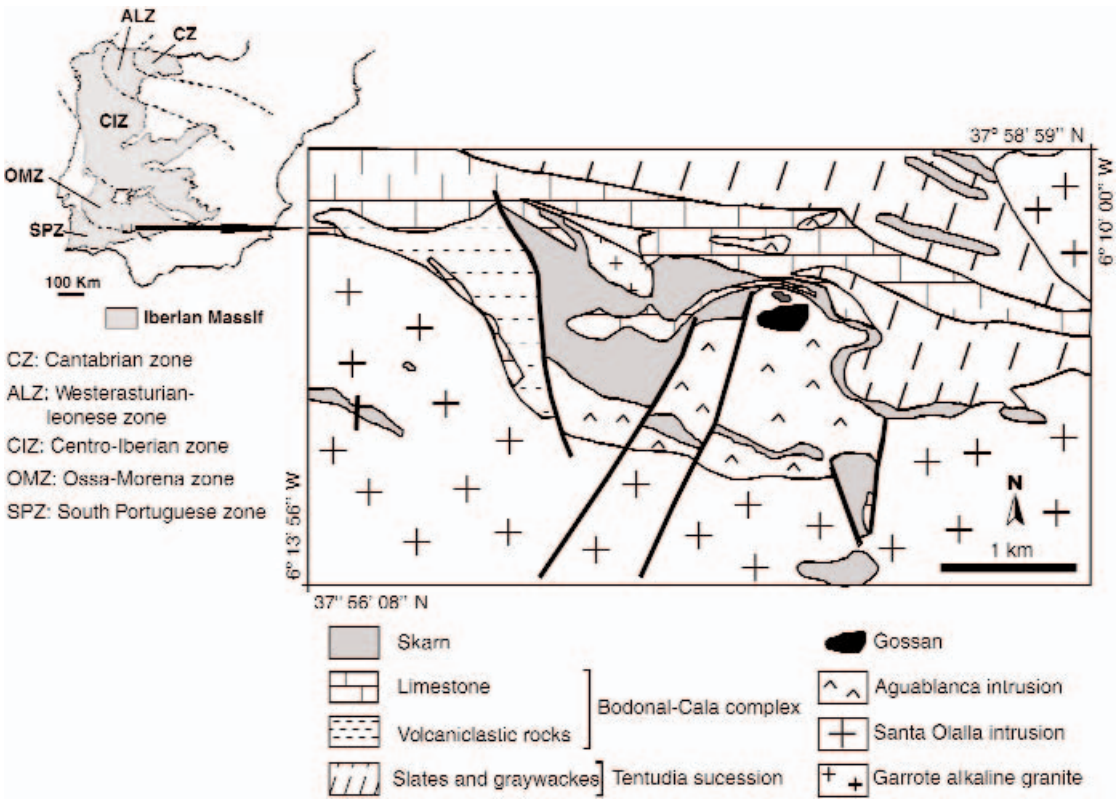

FIG. 1. Location of the Aguablanca deposit in the Iberian Massif. The outlined area is shown in detail in a schematic geologic map of the Aguablanca area. The mineralized zone is indicated by the gossan in the northern part of the Aguablanca intrusion.

of the European pre-Mesozoic Variscan chain. The Ossa-Morena zone is the result of a complex geodynamic evolution. During the Cadomian orogeny (620–480 Ma), the Ossa-Morena zone evolved as a continental magmatic arc, giving rise to calc-alkaline magmatism with the formation of dioritic-tonalitic rocks and anatectic granites throughout the northern and central sectors of the Ossa-Morena zone, respectively (Sánchez Carretero et al., 1990). During the Cambrian and Ordovician, an episode of intracontinental rifting gave rise to the formation of new ocean crust. This event was accompanied by extensive bimodal alkaline magmatism (Sánchez García et al., 2003). Subsequently, the zone evolved as a passive margin with the formation of Cambrian to Lower Permian volcanosedimentary, terrigenous, and carbonate sequences that underwent the Hercynian orogeny (390–300 Ma) (Eguiluz et al., 2000, and references therein). During this orogeny, an Andean-type magmatic arc with a large volume of calc-alkaline plutonic rocks developed. Radiometric data have given ages of crystallization for the ore-bearing Aguablanca intrusion of 338.6 ± 0.8 Ma (U-Pb in zircon: Romeo et al., 2004) and 338 ± 3 Ma (^{40}Ar-^{39}Ar in phlogopite: Tornos et al., 2004), indicating that this igneous body was coeval with the development of the Andean-type active margin during the Hercynian orogeny.

The Aguablanca pluton intrudes a series of interlayered volcanic graywackes and pyrite-bearing black slates (Tentudia succession, upper Precambrian) unconformably overlain by rhyolitic and dacitic volcanic and volcaniclastic rocks with carbonate rocks at the top (Bodonal-Cala complex, upper Precambrian-Lower Cambrian: Eguiluz et al., 2000; Fig. 1). The Tentudia succession represents the top of the Serie Negra, the distinctive 3,000-m-thick Precambrian series of the Ossa-Morena zone, mostly made up of black slates and quartzites. The Aguablanca intrusion is bounded to the south by the Santa Olalla pluton (Fig. 1), a calc-alkaline intrusive body with reverse compositional zoning. Amphibole-biotite quartz diorites merge into tonalite and monzogranite toward the center of the pluton (Casquet, 1980). The crystallization age of the Santa Olalla intrusion (341 ± 3 Ma, U-Pb in zircon: Romeo et al., 2004) is similar to that of Aguablanca pluton. Both intrusions produced a well-developed contact metamorphic aureole, mainly in the Bodonal-Cala carbonate rocks, with the formation of garnetite, calc-silicate rocks, and marble (Casquet, 1980).

The Aguablanca intrusion

This intrusion comprises a subcircular mafic body, approximately 3 km^2 in area (Fig. 1). A lithological study of the scarce outcrops and drill-core samples has identified different rock types characterized by cumulate textures: hornblende-bearing gabbronorite and minor gabbro, norite, and quartz-diorite. Most rocks of the intrusion contain no Fe-Ni-Cu sulfides, although small disseminations can be found where the igneous rocks envelope partially digested xenoliths of country sedimentary rocks. In places, minor mafic fragments (e.g., gabbro) are found. Hornblende-bearing gabbronorite is by far the most common rock type. It is a medium- to coarse-grained meso- and orthocumulate containing variable amounts of orthopyroxene (27–48 modal %), plagioclase (23–47%), clinopyroxene (4–11%), amphibole (10–21%), phlogopite (<5%), and minor interstitial quartz (<1%) (Fig. 2A). Locally, orthopyroxene or clinopyroxene are very minor, giving rise to gabbro and norite, respectively. Orthopyroxene and clinopyroxene are invariably cumulus minerals. Orthopyroxene occurs as prismatic euhedral to subhedral crystals (Fig. 2A) and clinopyroxene as larger subhedral crystals. Gabbronorites show subhorizontal layering at the decimeter scale, consisting of variations in the plagioclase modal contents. In the most leucocratic rocks, plagioclase forms cumulus tabular crystals, whereas in the most melanocratic rocks, plagioclase occurs as subhedral grains interstitial to pyroxenes (Fig. 2A). Green-brown amphibole and phlogopite are postcumulus, often including poikilitic pyroxene and plagioclase (Fig. 2A). Quartz-diorite occurs as variably thick masses

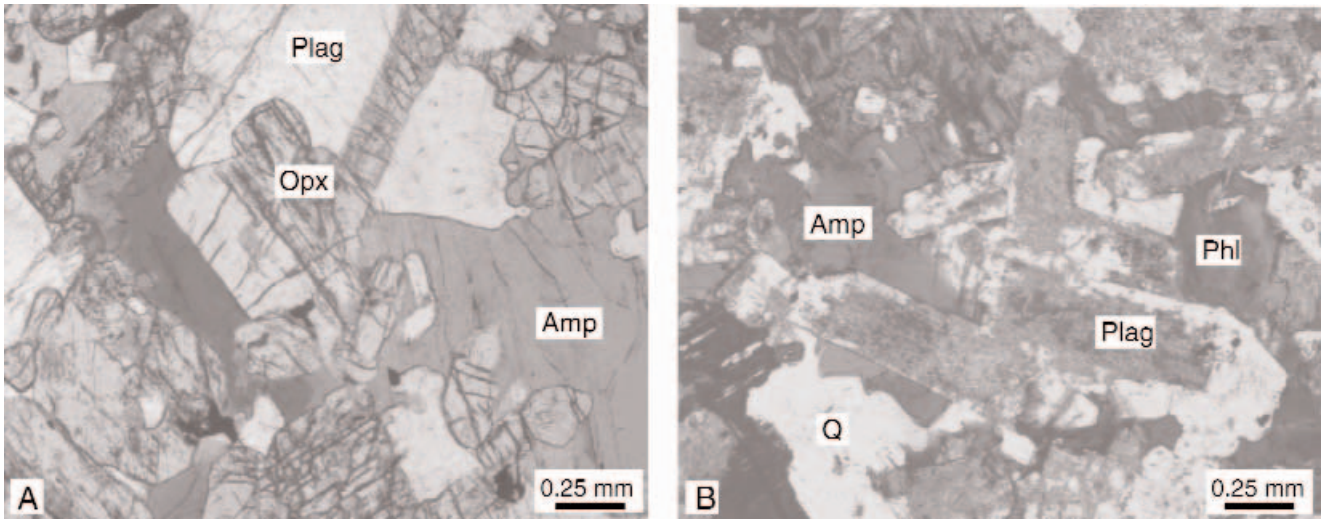

FIG. 2. Photomicrographs (transmitted light) of rocks from the main Aguablanca intrusion. A. Gabbronorite showing euhedral orthopyroxene crystals and poikilitic, intercumulus amphibole enclosing small cumulus crystals of plagioclase. B. Quartz-diorite with partially sericitized, cumulus plagioclase and postcumulus amphibole, phlogopite, and quartz. Abbreviations: amp = amphibole, Opx = orthopyroxene, phl = phlogopite, plag = plagioclase, Q = quartz.

(up to 150 m) between gabbronorite with transitional contacts. The quartz-diorite is composed of cumulus plagioclase (56–63%) with a lesser amount of cumulus clinopyroxene (<14%, but commonly below 5%) and orthopyroxene (<7%). Phlogopite (7–18%), quartz (5–15%), and amphibole (<7%) are postcumulus phases (Fig. 2B). The primary mineralogic assemblages are variably altered to a secondary assemblage comprising actinolite, chlorite, bastite, talc, carbonates, serpentine, albite, sericite, and epidote-zoisite group minerals, owing to the circulation of postmagmatic hydrothermal fluids.

The Ni-Cu Sulfide Deposit

The Ni-Cu sulfide mineralization is closely related to a magmatic breccia situated near the northern boundary of the Aguablanca intrusion. The breccia is poorly exposed at the surface, but drill core shows that it is well developed from a few meters below the surface to more than 600 m deep (Fig. 3). It has the shape of a subvertical funnel with a dip of 70º to 80º N. It is about 250 to 300 m wide (north-south) and 600 m long (east-west) (Fig. 3). Within the breccia, the mineralization is concentrated mainly in subvertical orebodies that are truncated by northeast-oriented, postmineralization faults (Fig. 3). Surface evidence of the sulfide deposit is an 8- to 10-m-thick gossan.

The breccia consists of a matrix of hornblende- and phlogopite-rich gabbronorite containing Ni-Cu-Fe sulfides which hosts barren or slightly mineralized mafic-ultramafic fragments (Fig. 4). In the gabbronorite matrix, mineralization occurs mostly as semimassive and disseminated sulfides (Fig. 4A, B). The semimassive ore consists of "leopard-textured" sulfides (Evans-Lamswood et al., 2000), up to 85 modal percent but more commonly between 20 and 70 percent. This texture comprises black spots of idiomorphic to subidiomorphic silicates (mostly pyroxene, olivine, and/or plagioclase) enclosed in a yellowish groundmass of sulfides (Figs. 4A, 5A). In the more abundant disseminated ore, sulfides (≤20 modal %) occur as polymineralic aggregates of variable grain size interstitial to the silicate framework (Fig. 5B). In general, the semimassive ore occurs in the core of the breccia surrounded by the disseminated ore and hosting more abundant fragments of mafic rocks (Fig. 3). The disseminated, ore-bearing gabbronorite grades outward laterally without systematic changes in the silicate mineralogy to sulfide-free gabbronorite, which locally contains some mafic-ultramafic fragments. Within the fragments, sulfides may occur as low-grade disseminations and as chalcopyrite veinlets which cut both fragments and host rocks.

The ore mineralogy has been described in detail by Ortega et al. (2000, 2004), who observed two mineral assemblages: (1) a subsolidus, reequilibrated magmatic assemblage, comprising pyrrhotite, pentlandite, chalcopyrite, and minor PGM (merenskyite, michenerite, palladian melonite, moncheite, and sperrylite), magnetite, ilmenite, Bi-, Ag-tellurides (tellurobismuthite, volinskyite, and hessite), and native gold; and (2) a hydrothermal assemblage, consisting of several textural types of pyrite.

The magmatic assemblage in the semimassive ore is characterized by coarse equant crystals of hexagonal pyrrhotite in

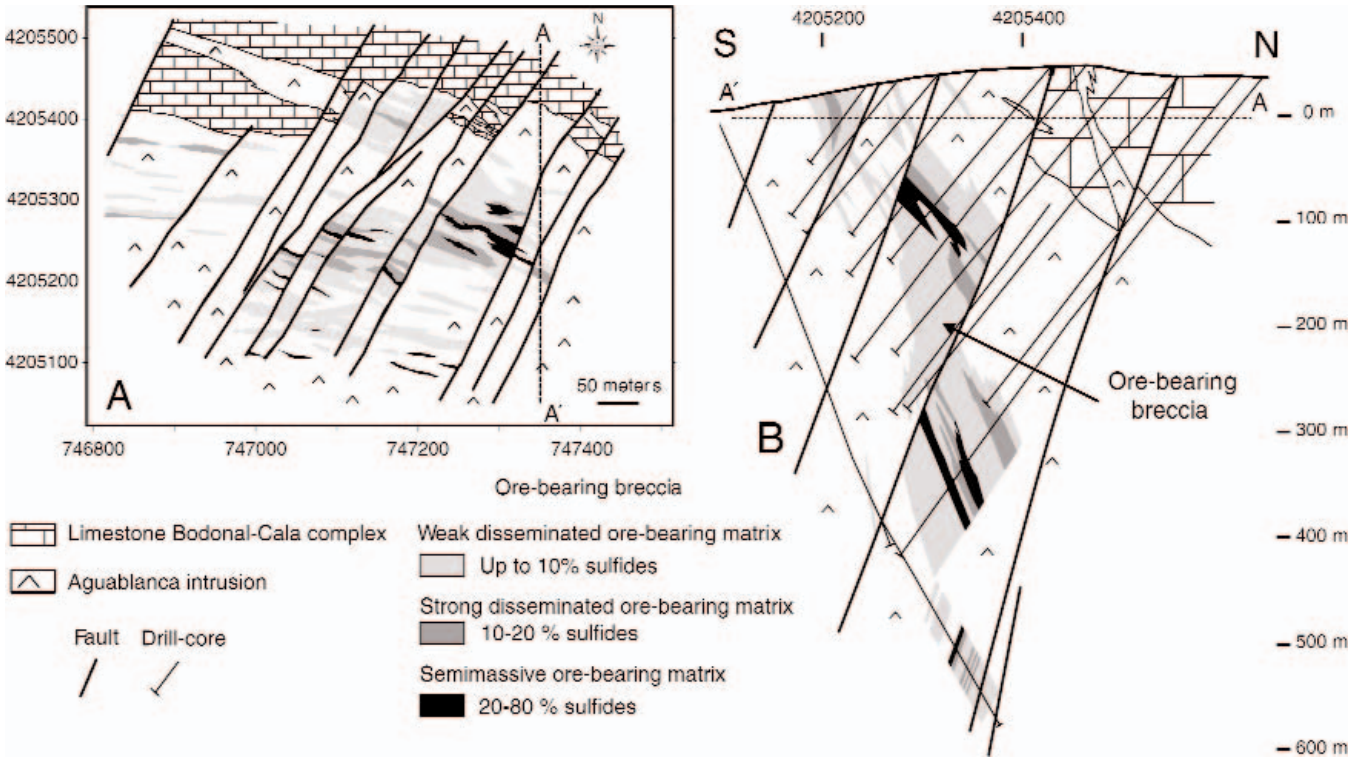

FIG. 3. A. Simplified map of the ore-bearing breccia in the Aguablanca intrusion based on drill core data. Fragments are irregularly distributed in the mineralized matrix, but they are more abundant in the matrix of the semimassive ore. Transverse cross section [A-A'] is shown in B. B. North-south–oriented transverse section across the ore-bearing breccia, based on drill-core information.

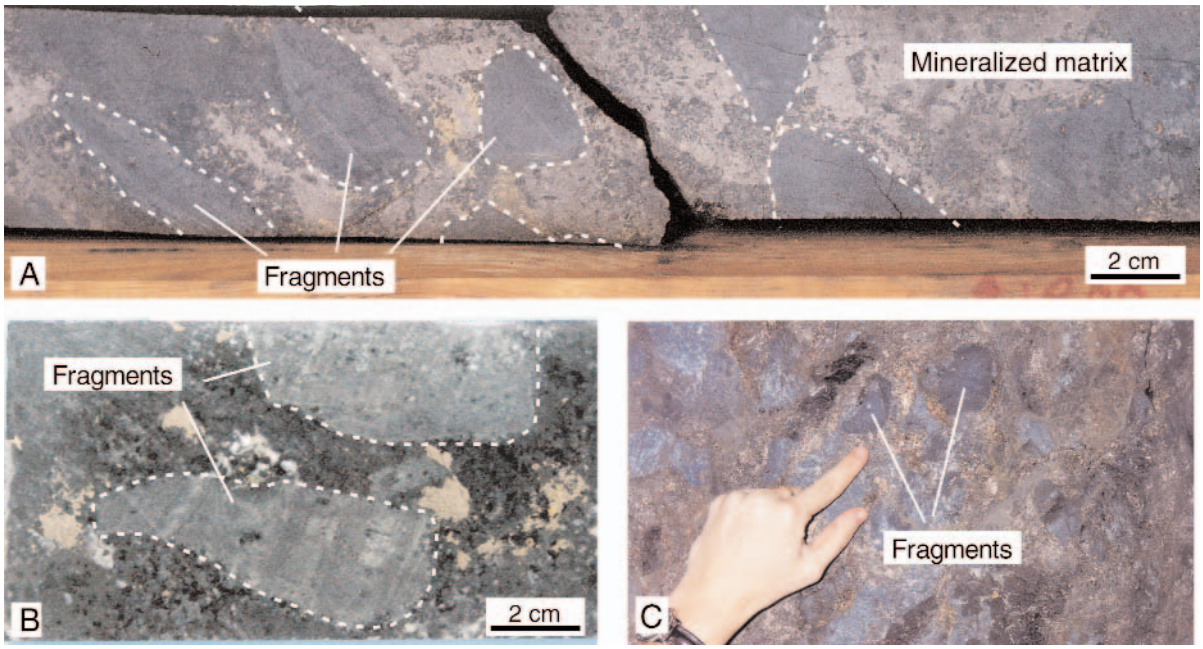

FIG. 4. A, B. Photographs of drill core showing the ore-bearing breccia. Barren, mafic fragments are hosted by a matrix containing semimassive (A) and disseminated (B) sulfides. C. Ore-bearing breccia exposed in an underground exploration gallery showing the barren fragments within a mineralized matrix.

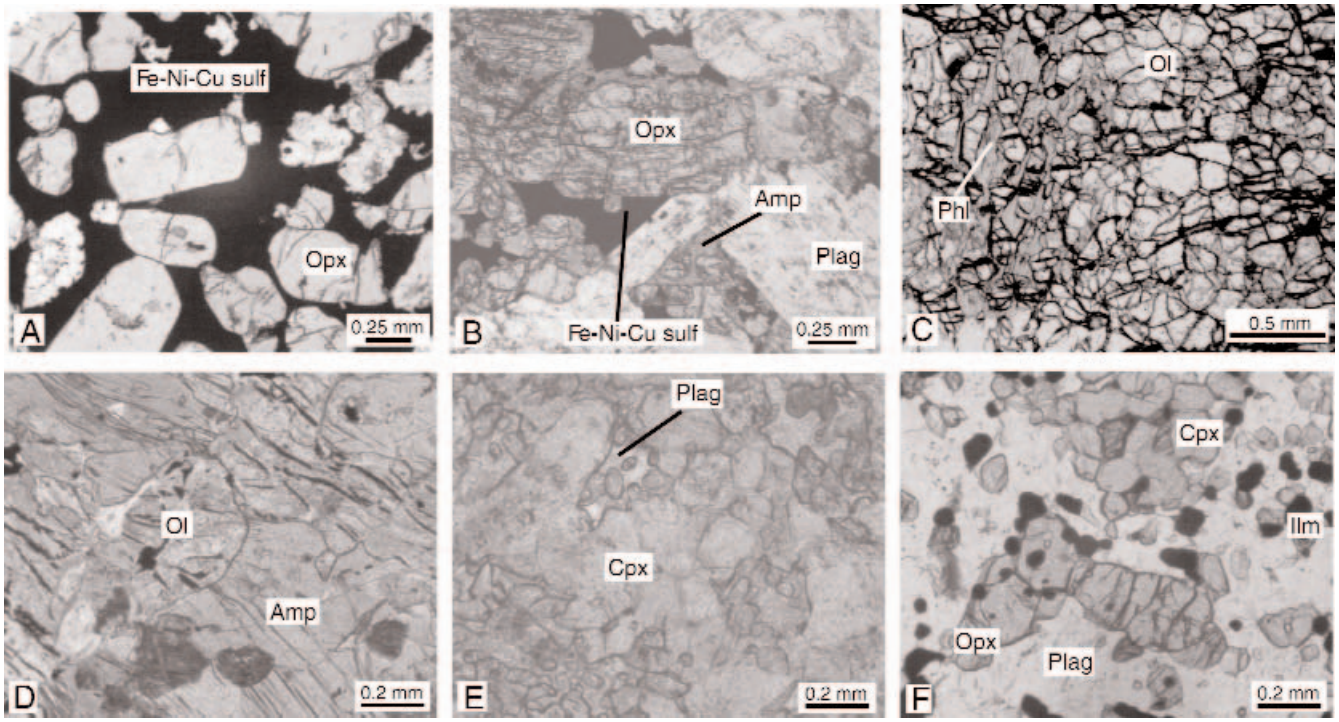

FIG. 5. Photomicrographs (transmitted light) of the ore-bearing matrix and the cumulate fragments from the breccia: A. Semimassive sulfides enveloping cumulus orthopyroxenes. B. Disseminated sulfides in gabbronorite with cumulus orthopyroxene and plagioclase with minor intercumulus amphibole. C. Cumulus olivine with poikilitic phlogopite in adcumulate of dunite. D. Serpentinized cumulus olivine in textural equilibrium with intercumulus amphibole in hornblende-rich harzburgite with orthocumulate texture. E. Cumulus clinopyroxene grains with triple-point contacts with interstitial plagioclase in gabbro. F. Fine-grained cumulus crystals of orthopyroxene, clinopyroxene, plagioclase and ilmenite in gabbronorite. amp = amphibole, cpx = clinopyroxene, il = Ilmenite, ol = olivine, opx = orthopyroxene, phl = phlogopite, plag = plagioclase.

mosaic aggregates with sparse flame exsolutions of pentlandite, surrounded by polycrystalline, chainlike pentlandite aggregates and minor interstitial chalcopyrite. The assemblage also includes euhedral crystals of Cr-bearing magnetite and ilmenite, notably related to the areas where the amount of sulfide is very high. The disseminated sulfides are mineralogically and texturally similar to the semimassive sulfides, although they have higher proportions of chalcopyrite and less pentlandite. Chalcopyrite veinlets and composite veinlets containing pyrrhotite and pentlandite cut both disseminated and semimassive sulfides as well as the silicate fragments. PGM are mainly associated with the sulfides, mostly within pentlandite, pyrrhotite, and, to a lesser extent, chalcopyrite, or close to the contacts between them. The PGM are considered to be the result of the partition of PGE in the immiscible sulfide liquid and the subsequent exsolution of Pt and Pd during the low-temperature reequilibration of the magmatic sulfide phases (Ortega et al., 2004; Piña et al., 2005).

The hydrothermal assemblage consists of pyrite, either replacing pyrrhotite and/or crosscutting the pyrrhotite-pentlandite-chalcopyrite assemblage, and is more abundant in areas with strong microfracturing. Textural features and Co/Ni ratios allow the identification of three main generations of pyrite, all formed by the circulation of postmagmatic fluids, coeval with the subsolidus recrystallization and the overall cooling of the deposit (Ortega et al., 2004).

Petrography of the Ore-Bearing Breccia

The abundant mafic-ultramafic fragments in the ore-bearing breccia have subangular to rounded shapes, sharp contacts with the mineralized matrix, and a size ranging from few to 8 cm (Fig. 4). Fragments typically do not show evidence of interaction with the host matrix, with the exception of some dunite fragments which have reaction rims with a higher concentration of hydrous phases such as chlorite, amphibole, and serpentine at the edges of the fragments. In places, growth of pyroxene and plagioclase laths in the gabbronorite matrix appears to have nucleated on the fragments. Individual fragments are usually composed of a single rock type, although a composite fragment of clinopyroxenite and anorthosite with sharp contacts between them also was observed.

Fragments are fine- to medium-grained and show typical microscopic cumulate textures. The magmatic mineralogic association includes olivine, orthopyroxene, clinopyroxene, plagioclase, amphibole, phlogopite, and opaque minerals (Cr-free spinel, magnetite, ilmenite, and minor Fe-Ni-Cu sulfides). The modal mineralogy of the fragments reveals a wide variety of rock types (Table 1): peridotite (dunite, harzburgite, and werhlite, representing 17% of 34 studied fragments), pyroxenite (orthopyroxenite and clinopyroxenite, 9%), gabbro (gabbro, hornblende gabbro, and gabbronorite, 60%), and anorthosite (14%). Gabbro is by far the main type of fragment. The gabbro fragments commonly exhibit the least sharp boundaries and the most rounded shapes. Petrographic descriptions of the fragments are summarized in Table 1 and illustrated in Figure 5. Fragments are commonly depleted in Fe-Ni-Cu sulfides, although some (e.g., harzburgite or gabbro) host very minor disseminations interstitial to primary silicates or in association with secondary minerals such as epidote or actinolite. Poikilitic textures are common, especially in peridotite fragments (Fig. 5C, D). Fine grain sizes and mosaic textures, characterized by mutual interference boundaries and triple junctions, are notable in fragments of dunite, orthopyroxenite, gabbro, and gabbronorite (Fig. 5C, E). Some fragments of gabbro exhibit microscopic grain sizes and cryptic layering in the cumulus clinopyroxene, and gabbronorite fragments show a well-developed igneous lamination in the cumulus plagioclase.

The gabbronorite matrix of breccias containing semimassive sulfides has a primary silicate assemblage of orthopyroxene (<48 modal %), plagioclase (<37 modal %), clinopyroxene (<25 modal %), and serpentinized olivine (<10 modal %). They occur as early-formed, medium-grained cumulus crystals (Fig. 5A). Plagioclase crystals are irregularly altered to sericite and show replacement by pyrite along grain boundaries (Ortega et al., 2004). Magmatic sulfide inclusions (mainly pyrrhotite and chalcopyrite) in plagioclase crystals give them a turbid appearance. Locally, sulfides also fill fractures in plagioclase. Embayed orthopyroxene grains and minor olivine crystals are locally included in clinopyroxene oikocrysts. Hornblende and phlogopite are present as postcumulus phases between cumulus silicates and sulfides.

The gabbronorite matrix of breccias containing disseminated sulfides is mostly medium-grained, meso- and orthocumulates of hornblende-bearing gabbronorite with minor gabbro, norite, gabbrodiorite, and hornblende pyroxenite. These rocks are mineralogically and texturally very similar to those of the main Aguablanca intrusion, showing the same alteration assemblage. The primary silicates include orthopyroxene (19–56 modal %), plagioclase (<52 modal %), clinopyroxene (<22 modal %), amphibole (<46 modal %), phlogopite (<14 modal %), and minor interstitial quartz. Orthopyroxene is cumulus, occurring as euhedral to subhedral medium-grained crystals (Fig. 5B), whereas clinopyroxene is commonly larger and less abundant than the coexisting orthopyroxene, as in the main intrusion. Clinopyroxene forms subhedral to anhedral cumulus grains that locally include orthopyroxene and, more rarely, plagioclase. Plagioclase occurs as cumulus grains and less commonly as an intercumulus phase between early-crystallized pyroxenes. Hornblende and phlogopite occur interstitially to pyroxene and plagioclase, locally with poikilitic textures. Orthopyroxene in contact with intercumulus amphibole or phlogopite exhibits embayed textures related probably to reactions between orthopyroxene and intercumulus liquid.

In summary, the sulfide content is the essential difference between the semimassive and disseminated ore, since the textures and mineralogy of the primary silicates are very similar throughout.

Mineral Chemistry

Mineral compositions were determined on polished thin sections using a JEOL Superprobe JXA-8900 M (15 Kv, 20 nA, 1–5-μm-beam diam) in the "Luis Bru" Centro de Microscopía Electrónica of the University Complutense of Madrid, Spain, and a JEOL Superprobe JXA-733 (15 Kv, 15 nA, and beam diam of 10 μm) in the Institute of Electron Optics of the University of Oulu, Finland.

Compositional ranges of the primary silicates from fragments, ore-bearing matrix, and unmineralized rocks of the

TABLE 1. Petrography of the Mafic-Ultramafic Fragments in the Aguablanca Ore-Bearing Breccia

Rock type	Cumulus minerals[1]	Intercumulus minerals	Textural characteristics
Dunite	Olivine (96–90) and Cr-free spinel (<10)	Phlogopite (<4), carbonates (<2), amphibole, plagioclase, orthopyroxene, clinopyroxene and sulfides (tr)	Fine-grained adcumulate; olivine forms fractured, rounded to subhedral crystals (<0.7 mm); Cr-free spinel occurs as green, euhedral crystals intergrown with or included in olivine; sharp boundaries between olivine and intercumulus, locally poikilitic, phlogopite
Hornblende-rich werhlite	Olivine (56) and Cr-free spinel (2)	Clinopyroxene (24), plagioclase (10), amphibole (7) and phlogopite (1)	Medium-grained orthocumulate; olivine occurs as rounded to subrounded grains (0.3–2 mm) enclosed by poikilitic clinopyroxene; olivine shows sharp boundaries with intercumulus clinopyroxene and amphibole, suggesting no replacement reaction between them; Cr-free spinel is enclosed in intercumulus plagioclase
Hornblende-rich harzburgite	Olivine (43), orthopyroxene (18) and Cr-free spinel	Amphibole (25), plagioclase (8), sulfides (5) and phlogopite (1)	Medium-grained orthocumulate, olivine occurs as rounded crystals (0.15–1.25 mm) and orthopyroxene as subhedral grains (1–2.5 mm), both locally included in poikilitic amphibole; Cr-free spinel form fine-grained, anhedral crystals within intercumulus plagioclase
Orthopyroxenite	Orthopyroxene (>98)	Phlogopite (<2) and sulfides (tr)	Fine-grained adcumulate; orthopyroxene exhibits straight or slightly curved grain boundaries and has an uniform size (<0.3 mm) and 120º triple junctions
Clinopyroxenite	Clinopyroxene (88–86)	Plagioclase (8–4), phlogopite (8–3) and amphibole (<3)	Meso- to adcumulate; clinopyroxene forms anhedral grains (0.5–1.2 mm) linked by triple-point junctions; intercumulus plagioclase, phlogopite, and amphibole locally enclose clinopyroxenes
Gabbro (cumulus clinopyroxene)	Clinopyroxene (85–36) and orthopyroxene (<2)	Plagioclase (50–15), amphibole (<16), phlogopite (<9), sulfides (<5), carbonates and quartz (tr)	Fine-grained meso- and orthocumulate; clinopyroxene ocurs as anheral crystals (<0.2 mm) with triple-point contacts, forming a mosaic texture with mutual interference boundaries; plagioclase and less frequently amphibole and phlogopite show poikilitic texture enclosing small and rounded clinopyroxene grains (<0.05 mm)
Gabbro (intercumulus clinopyroxene)	Plagioclase (35–33)	Clinopyroxene (63.0–55.5), amphibole (<2.5), sulfides (<7) and phlogopite (tr)	Mesocumulate; plagioclase consists of tabular grains (0.4 mm) coexisting in equilibrium with postcumulus clinopyroxene; phlogopite and amphibole form large poikilitic crystal
Gabbronorite	Plagioclase (64–56), orthopyroxene (25–8), clinopyroxene (22–7) and ilmenite (<12)	Sulfides (<3), amphibole, and phlogopite (tr)	Fine-grained adcumulate; plagioclase, orthopyroxene and clinopyroxene form euhedral to subhedral crystals and commonly show triple-junctions; ilmenite, if present, occurs as euhedral crystals intergrown with plagioclase, orthopyroxene, and clinopyroxene
Hornblende gabbro	Plagioclase (49) and amphibole (45)	Phlogopite (5) and sulfides (tr)	Plagioclase forms euhedral to subhedral crystals in equilibrium with amphibole; phlogopite occurs interstitially between plagioclase and amphibole and as inclusions in amphibole
Anorthosite	Plagioclase (84–73), orthopyroxene (<7), clinopyroxene (<4) and olivine (<3)	Amphibole (<6), phlogopite (<6) and sulfides (<2)	Fine- to medium-grained adcumulate; plagioclase occurs as subhedral crystals (0.5–1.5 mm) with mutual interference boundaries and common triple-junctions; Cr-free spinel forms equant grains associated with magnetite and ilmentite and between plagioclase; orthopyroxene is commonly cumulus; olivine occurs as small inclusions in plagioclase

[1] Numbers in brackets refer to modal proportions; tr = trace amount (<1%)

main Aguablanca intrusion are summarized in Table 2. Representative analyses of olivine, clinopyroxene, orthopyroxene, plagioclase, amphibole, and phlogopite are listed in Tables 3 and 4. The magnesium content of olivine, orthopyroxene, clinopyroxene, amphibole, and phlogopite are expressed as Mg no. = (Mg/Mg+Fe), calculated from cationic proportions.

Olivine

Forsterite (Fo) content (= 100 Mg no.) of olivine in the fragments ranges between 79 and 91. The highest Fo contents are observed in the peridotite fragments (90–91 in hornblende-rich werhlite, 83–88 in dunite, and 84 in hornblende-rich harzburgite). In anorthosite, olivine has the lowest Fo contents (79–81). MnO contents range from 0.14 to 0.40 wt percent, CaO never exceeds 0.11 wt percent, and NiO is always below 0.25 wt percent, with the most Mg enriched olivines containing Ni below the detection limit of the microprobe. No analyses could be obtained of olivine in the gabbronorite matrix of the breccia because of its extensive serpentinization.

TABLE 2. Summary of the Compositional Characteristics of the Primary Silicates in the Fragments, Ore-Bearing Matrix, and Rocks of the Main Aguablanca Intrusion

Rock type	100 Mg# ol	Mg# opx	Mg# cpx	%An plg	Mg# amp	Mg# phl
Fragments						
Dunite	83–88	0.84–0.85	0.91	85	0.82–0.85	0.88–0.89
Hbl-rich werhlite	90–91		0.90–0.93	81–88	0.83–0.87	
Hbl-rich harzburgite	84	0.82		90	0.76–0.79	0.85–0.87
Orthopyroxenite		0.80				
Clinopyroxenite			0.83–0.85	47–55	0.80	0.74–0.75
Gabbro (Cpx cumulus)		0.77–0.81	0.72–0.89	45–99	0.68–0.81	0.73–0.76
Gabbro (Cpx intercumulus)			0.62–0.80	92–97		0.76
Gabbronorite		0.73–0.81	0.78–0.84	67–78	0.68–0.83	0.69
Hbl gabbro				38–57	0.72–0.77	0.78
Anorthosite	79–81	0.76–0.80	0.83–0.87	50–84	0.68–0.81	0.64–0.84
Ore-bearing matrix						
Disseminated ore		0.74–0.83	0.78–0.89	47–77	0.70–0.86	0.69–0.84
Semimassive ore		0.77–0.85	0.78–0.88	50–89	0.73–0.79	0.72
Aguablanca intrusion						
Gabbronorite		0.78–0.85	0.83–0.89	51–79	0.74–0.85	0.73–0.79
Quartz-diorite		0.62–0.67	0.73–0.77	37–45	0.75–0.78	0.60–0.63

Mg# = Mg/(Mg+Fe), An = Ca/(Ca+Na+K); both calculated from cationic proportions; Cpx = clinopyroxene, ol: olivine, opx = orthopyroxene, = cpx: clinopyroxene, plg = plagioclase, amp = amphibole, phl = phlogopite, hbl = hornblende

Clinopyroxene

Clinopyroxene in the fragments is mostly diopside ($Wo_{51–45}En_{46–31}Fs_{18–4}$), although some grains fall in the diopside-augite series. Intercumulus clinopyroxene in the hornblende-rich werhlite shows the most primitive compositions, with Mg no. ranging from 0.90 to 0.93. In clinopyroxenite, gabbro, and gabbronorite fragments, clinopyroxene encompasses a wide range of compositions (Mg no. = 0.72–0.89). In the gabbro fragments, intercumulus clinopyroxene shows Mg no. from 0.62 to 0.80. In anorthosite, Mg no. ranges from 0.83 to 0.87. Major and minor element contents in clinopyroxene from the gabbro and clinopyroxenite fragments vary systematically with Mg no., with an overall decrease in SiO_2 and an increase in Al_2O_3 and TiO_2 contents with decreasing Mg no. (Fig. 6). $Na_2O + K_2O$ variation is characterized by a steady decrease in the more Fe enriched intercumulus clinopyroxene, likely related to the early crystallization of plagioclase in these rocks at cumulus phase, decreasing considerably the alkali content of the residual liquid from which clinopyroxene formed.

Clinopyroxene in the gabbronorite matrix of semimassive and disseminated ore-bearing breccias has an Mg no. ranging from 0.78 to 0.89. As a whole, clinopyroxene from the gabbronorite matrix is more primitive than clinopyroxene in the fragments; it commonly has higher Cr_2O_3 content (up to 0.75 wt %, averaging 0.28 wt %) and lower Al_2O_3 (<3 wt %) and TiO_2 (<0.6 wt %) contents than in the fragments (Cr_2O_3 contents rarely exceed 0.2 wt %, and Al_2O_3 and TiO_2 contents are as high as 5 to 6 wt % and up to 1 wt %, respectively: Table 3). Compositionally, clinopyroxene from gabbronorites and quartz-diorites of the main Aguablanca intrusion is similar to that in the gabbronorite matrix of the breccias, with Mg no. oscillating between 0.83 to 0.89 and 0.73 to 0.77, respectively (Table 2).

Orthopyroxene

Orthopyroxene is enstatite in all fragments with a compositional range of $Wo_{1–2}En_{71–82}Fs_{17–24}$. It is relatively poor in Al_2O_3 (<3 wt %) and TiO_2 (<0.4 wt %), and has variable CaO (0.30–1.60 wt %) and SiO_2 (52–56 wt %) contents. Cr_2O_3 contents are commonly below 0.21 wt percent. Orthopyroxene shows an Fe-enrichment trend in the fragments; Mg no. progressively decreases from peridotite (0.85–0.82) to orthopyroxenite (0.80), anorthosite (0.80–0.76), and gabbroic rocks (0.81–0.73). Olivine and orthopyroxene compositions are well correlated in those rocks where they coexist, suggesting that they were in equilibrium (Féménias et al., 2003).

In the gabbronorite matrix, orthopyroxene is compositionally similar to that of the fragments (Mg no. = 0.85–0.74), although it is slightly more enriched in Mg in the gabbronorite associated with semimassive sulfides ($Wo_{2.3}En_{78.9}Fs_{18.8}$) than in the gabbronorite associated with disseminated sulfides ($Wo_{1.8}En_{77.3}Fs_{20.9}$). The Mg no. in orthopyroxene from gabbronorites and quartz-diorites of the main Aguablanca intrusion ranges from 0.85 to 0.78 and 0.67 to 0.62, respectively.

Plagioclase

Plagioclase compositions in the fragments vary from An_{99} to An_{38}. Peridotite fragments contain unzoned, postcumulus plagioclase with compositions from An_{81} to An_{90}. The composition of postcumulus plagioclase in gabbro fragments varies from labradorite to anorthite (An_{50} to An_{99}). In gabbronorite and anorthosite fragments, cumulus plagioclase is high in An, from An_{68} to An_{78} in gabbronorite and from An_{51} to An_{85} in anorthosite. The most sodic plagioclase (An_{38} to An_{57}) occurs in hornblende gabbro.

Individual grains of plagioclase in the gabbronorite matrix with semimassive sulfides are not compositionally homogeneous and display small anorthite-poor cores ($An_{50–60}$) with

TABLE 3. Representative Microprobe Analyses of Olivine, Orthopyroxene, and Clinopyroxene

Location	Mafic-ultramafic fragments													Ore-bearing matrix				Main Aguablanca intrusion			
Phase	Ol	Ol	Ol	Opx	Opx	Opx	Opx	Opx	Cpx	Cpx	Cpx	Cpx	Cpx	Opx	Opx	Cpx	Cpx	Opx	Opx	Cpx	Cpx
Rock type	Werh	Dunite	Anorth	Harz	Orthopy	Gabbro[1]	Anorth	Gnorite	Werh	Anorth	Gnorite	Gabbro[1]	Gabbro[2]	SM. ore	D. ore	SM. ore	D. ore	Gnorite	Q-diorite	Gnorite	Q-diorite
SiO_2	41.10	39.54	39.86	55.78	54.37	54.02	52.33	53.45	51.66	54.36	51.11	50.14	46.45	55.64	55.62	51.80	52.94	55.02	52.63	53.13	53.94
TiO_2	0.01	0.04	0.05	0.18	0.27	0.26	0.35	0.33	0.84	0.10	0.53	0.50	1.47	0.06	0.24	0.23	0.07	0.20	0.22	0.25	0.08
Al_2O_3	0.01	b.d.	b.d.	1.01	1.27	1.47	1.66	1.25	2.93	0.68	2.43	2.46	6.44	1.23	1.12	1.83	0.56	1.35	0.64	1.59	0.65
Cr_2O_3	n.a.	n.a.	n.a.	0.08	b.d.	0.04	0.03	0.00	b.d.	0.07	0.01	b.d.	b.d.	0.22	0.17	0.33	0.18	0.20	0.01	0.18	0.01
FeO	8.89	11.90	17.72	11.55	13.29	13.54	15.70	17.48	2.25	4.95	7.57	7.47	10.49	12.11	13.55	5.59	4.39	13.65	22.47	5.12	8.25
MnO	0.33	0.24	0.13	0.34	0.43	0.47	0.35	0.37	0.05	0.17	0.25	0.74	0.36	0.09	0.36	0.25	0.15	0.22	0.44	0.09	0.24
MgO	49.39	47.67	42.60	29.47	28.23	28.17	27.81	26.67	16.32	15.99	15.11	14.07	10.31	29.15	28.99	15.82	16.39	28.51	21.30	16.26	14.53
CaO	0.07	0.01	b.d.	1.20	1.27	1.26	1.17	0.78	25.36	24.32	22.27	23.40	23.81	0.84	0.68	23.13	24.41	0.58	1.32	22.29	23.12
Na_2O	0.01	0.01	b.d.	0.03	0.07	b.d.	0.02	0.01	0.10	0.20	0.30	0.41	0.13	0.00	0.02	0.21	0.16	0.01	0.03	0.29	0.28
K_2O	b.d.	0.02	b.d.	b.d.	0.05	0.00	0.01	0.01	0.02	0.02	b.d.	b.d.	b.d.	b.d.	b.d.	b.d.	b.d.	0.01	0.01	0.04	b.d.
NiO	b.d.	0.04	0.25	0.01	0.08	0.05	0.04	b.d.	b.d.	0.03	b.d.	b.d.	b.d.	0.11	b.d.	0.10	b.d.	0.10	0.03	0.06	b.d.
Total	99.80	99.45	100.62	99.65	99.33	99.27	99.47	100.35	99.52	100.89	99.59	99.19	99.46	99.45	100.74	99.29	99.24	99.84	99.08	99.30	101.10
Atomic concentration																					
Si	1.005	0.986	1.006	1.985	1.954	1.945	1.889	1.931	1.890	1.978	1.895	1.872	1.764	1.988	1.971	1.916	1.952	1.970	1.986	1.959	1.982
Al				0.042	0.054	0.063	0.071	0.053	0.130	0.030	0.106	0.108	0.239	0.052	0.047	0.080	0.024	0.056	0.028	0.069	0.028
Ti		0.001	0.001	0.005	0.007	0.007	0.010	0.009	0.020	0.003	0.015	0.014	0.042	0.002	0.006	0.006	0.002	0.005	0.008	0.007	0.002
Fe^{3+}					0.030	0.032	0.133	0.068	0.060	0.021	0.096	0.149	0.110			0.080	0.073			0.016	0.023
Fe^{2+}	0.182	0.248	0.374	0.344	0.369	0.376	0.341	0.460	0.010	0.130	0.139	0.085	0.223	0.362	0.402	0.093	0.062	0.409	0.709	0.142	0.230
Mg	1.800	1.772	1.603	1.564	1.513	1.512	1.497	1.436	0.890	0.868	0.835	0.783	0.584	1.552	1.532	0.873	0.901	1.522	1.198	0.894	0.796
Mn	0.007	0.005	0.003	0.010	0.013	0.014	0.011	0.011	0.002	0.005	0.008	0.023	0.011	0.003	0.011	0.008	0.005	0.007	0.014	0.003	0.007
Cr				0.002		0.001	0.001			0.002				0.006	0.005	0.010	0.005	0.006		0.005	
Ni		0.001	0.005		0.002	0.001	0.001			0.001				0.003		0.003		0.003	0.001	0.002	
Ca	0.002			0.046	0.049	0.049	0.045	0.030	0.990	0.949	0.885	0.936	0.969	0.032	0.026	0.917	0.964	0.022	0.053	0.881	0.910
K				0.001	0.002				0.001	0.001								0.001		0.002	
Na				0.002	0.005		0.002	0.001	0.007	0.014	0.022	0.030	0.010		0.001	0.015	0.011		0.002	0.021	0.020
Total	2.996	3.013	2.992	4.001	3.998	4.000	4.001	3.999	4.000	4.002	4.001	4.000	3.952	4.000	4.001	4.001	3.999	4.001	3.999	4.001	3.998
Mg#	0.91	0.88	0.81	0.82	0.80	0.79	0.76	0.73	0.93	0.85	0.78	0.77	0.64	0.81	0.79	0.83	0.87	0.79	0.63	0.85	0.76
Wo				2.33	2.47	2.46	2.23	1.51	50.86	48.09	45.08	47.37	51.07	1.65	1.31	46.58	48.10	1.13	2.69	45.50	46.27
En				79.65	76.62	76.26	73.85	71.60	45.54	44.00	42.56	39.63	30.76	79.65	77.75	44.33	44.93	77.67	60.68	46.19	40.47
Fs				18.02	20.91	21.29	23.92	26.89	3.60	7.91	12.36	13.00	18.16	18.70	20.94	9.10	6.98	21.20	36.63	8.31	13.26

All Fe as FeO, Mg# = (Mg/Mg+Fe), En = 100 Mg/(Mg+Fe+Mn+Ca), Fs = 100 Fe/(Mg+Fe+Mn+Ca), Wo = 100 Ca(Mg+Fe+Mn+Ca), Mg#, En, Fs, Wo calculated from cationic proportions, Werh = hornblende-rich werhlite, Anorth = anorthosite, Harz - hornblende-rich harzburgite, Orthpy = orthopyroxenite, Gnorite = gabbronorite, SM. ore = semimassive ore-bearing matrix, D. ore = disseminated ore-bearing matrix, n.a. = not analyzed, b.d. = below detection limits

[1] Gabbro = gabbro (cpx cumulus)

[2] Gabbro = gabbro (cpx intercumulus)

TABLE 4. Representative Microprobe Analyses of Plagioclase, Amphibole, and Phlogopite

Location	Mafic-ultramafic fragments													Ore-bearing matrix				Main Aguablanca intrusion				
Phase	Plag	Plag	Plag	Plag	Plag Hbl	Amp	Amp	Amp	Amp	Amp Hbl	Phl	Phl	Phl	Plag	Plag	Amp	Phl	Plag	Plag Q-	Amp	Phl	Phl Q-
Rock type	Werh	Anorth	Gnorite	Gabbro[1]	gabbro	Werh	Harz	Gabbro[1]	Gnorite	gabbro	Dunite	Harz	Gabbro[1]	SM. ore	SM. ore	D. ore	D. ore	Gnorite	diorite	Gnorite	Gnorite	diorite
SiO_2	45.59	48.82	49.32	44.57	56.54	40.76	43.58	41.73	41.19	43.67	36.41	37.91	36.33	54.90	49.17	48.46	36.51	48.68	57.10	47.88	37.39	37.38
TiO_2	0.03	b.d.	b.d.	0.04	0.02	4.48	0.31	3.65	4.04	3.13	1.65	2.89	2.89	0.09	0.02	1.16	5.06	0.04	0.04	1.50	5.57	3.52
Al_2O_3	34.01	33.15	31.20	35.43	26.22	13.82	12.55	11.79	11.21	10.46	16.99	15.42	15.16	28.86	33.22	6.46	14.21	33.19	27.19	7.79	14.56	14.41
Cr_2O_3	n.a.	n.a.	n.a.	n.a.	n.a.	b.d.	0.02	0.01	0.03	0.06	b.d.	0.54	0.62	n.a.	n.a.	0.51	0.82	n.a.	n.a.	0.66	0.38	0.45
FeO	0.22	0.21	0.26	0.18	0.24	4.26	8.73	8.96	11.39	10.20	5.31	6.49	10.97	0.23	0.24	8.42	9.62	0.27	0.07	8.06	10.64	14.94
MnO	b.d.	b.d.	b.d.	0.02	b.d.	0.13	0.14	0.08	0.11	0.11	0.06	0.10	0.03	b.d.	b.d.	0.06	0.05	b.d.	b.d.	0.07	0.04	0.10
MgO	0.02	0.00	0.02	b.d.	b.d.	15.91	16.59	14.84	13.38	14.44	22.30	20.49	16.93	0.03	b.d.	17.39	17.34	b.d.	b.d.	16.23	16.49	13.41
CaO	18.79	16.36	14.46	18.65	9.41	12.98	12.22	12.40	11.91	12.34	0.03	b.d.	0.02	11.20	16.21	12.05	b.d.	16.14	8.91	12.34	0.01	0.03
Na_2O	1.33	2.42	3.56	0.92	6.55	1.97	1.99	1.61	1.34	2.03	0.16	0.49	0.06	5.33	2.70	1.34	0.28	2.54	7.06	1.47	0.10	0.05
K_2O	0.05	0.05	0.12	0.05	0.26	1.06	0.89	1.18	1.21	0.86	9.18	9.01	9.60	0.15	0.08	0.55	9.52	0.07	0.04	0.16	7.77	7.94
Cl	n.a.	n.a.	n.a.	n.a.	n.a.	0.24	0.39	0.34	0.38	n.a.	0.52	0.33	0.60	n.a.	n.a.	0.33	0.55	n.a.	n.a.	0.23	0.39	0.43
F	n.a.	n.a.	n.a.	n.a.	n.a.	b.d.	0.14	0.17	b.d	n.a.	0.11	b.d.	0.09	n.a.	n.a.	0.18	0.09	n.a.	n.a.	0.04	0.05	0.07
Total	100.04	99.45	98.94	99.86	99.24	95.61	97.54	96.76	96.20	97.24	92.07	93.67	93.29	100.79	101.64	96.91	94.04	100.91	100.41	96.43	93.37	92.73
Atomic concentration																						
Si	2.108	2.215	2.280	2.062	2.566	6.023	6.269	6.169	6.173	6.424	5.616	5.799	5.755	2.461	2.218	7.006	5.713	2.211	2.555	6.959	5.815	5.979
Al^{IV}	1.768	1.771	1.698	1.930	1.401	1.977	1.731	1.831	1.827	1.576	2.384	2.201	2.245	1.523	1.765	0.994	2.287	1.775	1.433	1.041	2.185	2.021
Al^{VI}						0.428	0.394	0.221	0.152	0.237	0.702	0.577	0.583			0.105	0.331			0.292	0.482	0.694
Ti	0.001			0.001	0.001	0.498	0.033	0.406	0.456	0.347	0.191	0.332	0.345	0.003	0.001	0.127	0.595	0.001	0.001	0.164	0.651	0.424
Fe^{3+}							0.673	0.150	0.232	0.023						0.242				0.057		
Fe^{2+}	0.009	0.008	0.010	0.007	0.009	0.527	0.377	0.957	1.196	1.232	0.685	0.830	1.453	0.008	0.009	0.775	1.258	0.010	0.003	0.923	1.384	1.999
Mg			0.001			3.506	3.557	3.271	2.988	3.166	5.127	4.673	3.998	0.002		3.747	4.045			3.516	3.822	3.199
Mn	0.001			0.001		0.016	0.016	0.010	0.014	0.014	0.008	0.013	0.004			0.008	0.006			0.009	0.005	0.013
Cr							0.003	0.001	0.003	0.007		0.065	0.078			0.059	0.102			0.076	0.047	0.056
Ca	0.846	0.795	0.716	0.925	0.458	2.025	1.883	1.964	1.912	1.945	0.004	0.000	0.004	0.538	0.784	1.866	0.000	0.786	0.427	1.922	0.001	0.005
K	0.002	0.003	0.007	0.003	0.015	0.199	0.164	0.223	0.231	0.162	1.806	1.758	1.939	0.009	0.005	0.102	1.900	0.004	0.002	0.030	1.533	1.620
Na	0.196	0.213	0.319	0.083	0.576	0.565	0.556	0.462	0.390	0.579	0.047	0.145	0.018	0.463	0.236	0.376	0.084	0.224	0.613	0.415	0.030	0.016
Total	4.931	5.005	5.031	5.012	5.026	15.764	15.656	15.665	15.574	15.712	16.570	16.393	16.422	5.007	5.018	15.407	16.321	5.011	5.034	15.404	15.955	16.026
Cl						0.060	0.094	0.085	0.098		0.273	0.172	0.324			0.080	0.289			0.056	0.205	0.234
F						0.000	0.061	0.081	0.000		0.103		0.086			0.081	0.092			0.017	0.044	0.071
An	88	79	69	92	44									53	76.5			77	41			
Mg#						0.87	0.78	0.75	0.68	0.72	0.88	0.85	0.73			0.79	0.76			0.78	0.73	0.62

Atomic concentrations recalculated to 8, 23 and 24 oxygens for plagioclase, amphibole and phlogopite, respectively

All Fe as FeO; Mg# = (Mg/Mg+Fe), An = 100(Ca/Ca+Na), Mg# and An calculated from cationic proportion; Werh = hornblende-rich werhlite, Anorth = anorthosite, Harz = hornblende-rich harzburgite, Gnorite = gabbronorite, SM. ore = semimassive ore-bearing matrix, D. ore = disseminated ore-bearing matrix, n.a. = not analyzed; b.d. = below detection limits

[1] Gabbro = gabbro (cpx cumulus)

[2] Gabbro=gabbro (cpx intercumulus)

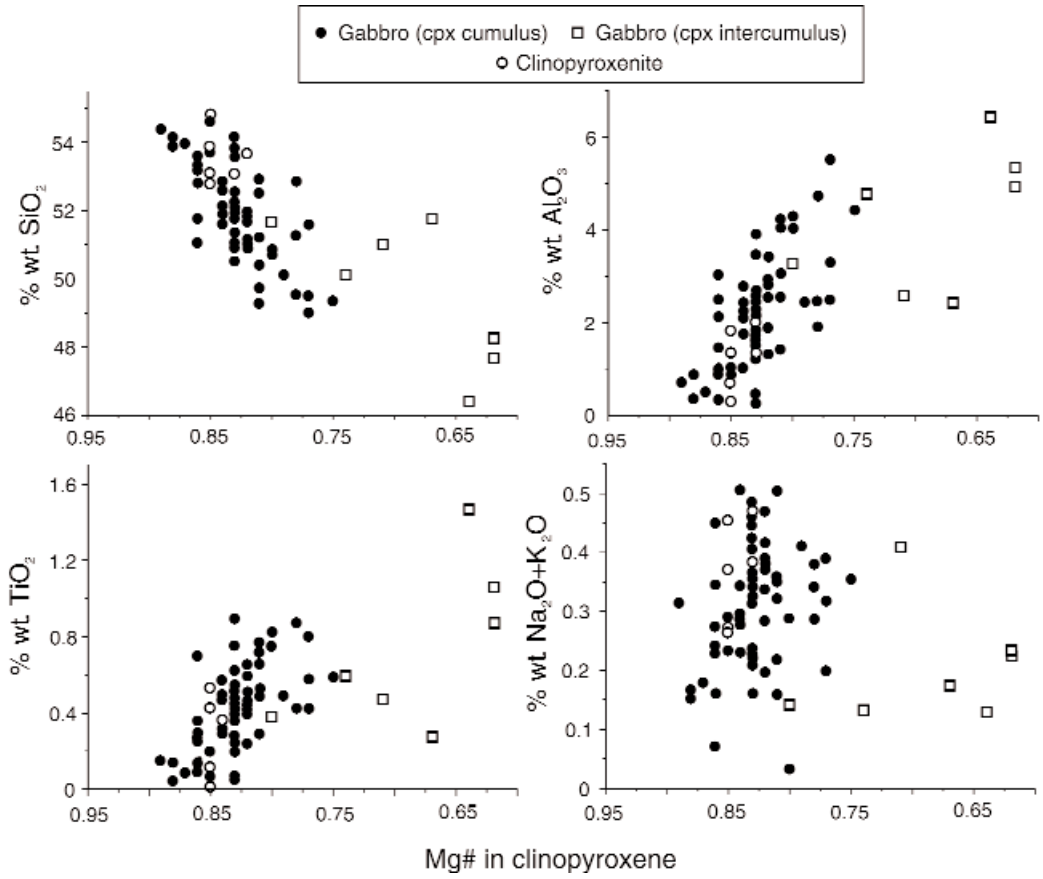

FIG. 6. Plots of SiO_2, Al_2O_3, TiO_2 and $Na_2O + K_2O$ versus Mg no. of clinopyroxene in the gabbro (with cumulus and intercumulus clinopyroxene) and clinopyroxenite fragments from the ore-bearing breccia. Points represent analyses of individual grains.

Ca-rich rims ($An_{74–88}$). Such reversely zoned plagioclases have been interpreted as a result of supercooling or abrupt loss of volatile from the magma (e.g., Berg, 1980; Mathison, 1987). In the gabbronorite and gabbrodiorite matrix of the disseminated, ore-bearing breccias, plagioclase varies from An_{47} to An_{81} and from An_{30} to An_{56}, respectively. Plagioclase in gabbronorites of the main Aguablanca intrusion ranges from An_{51} to An_{79}. In quartz-diorite, it is notably more evolved, from An_{37} to An_{45}.

Amphibole

Amphiboles in the peridotite fragments are mostly pargasite, pargasitic hornblende, and Mg hastingsite following the International Mineralogical Association (I.M.A.) nomenclature (Leake, 1978). In gabbro and gabbronorite, amphiboles cover a wide compositional range from pargasite to Mg hornblende, edenitic hornblende, Mg hastingsite, and edenite, whereas in hornblende gabbro, amphibole is dominantly pargasitic hornblende. Differentiation is marked by a decrease in Mg no. from peridotite fragments (0.76–0.87) to gabbronorite (0.68–0.83), gabbro (0.68–0.81), and hornblende gabbro (0.72–0.77). High contents of TiO_2 occur in the more Fe-enriched amphiboles (>2.5 wt %) relative to those with more primitive compositions (<1.5 wt %), typical of fractionated rocks (e.g., Snoke et al., 1981).

Postcumulus amphibole in semimassive ore is pargasitic hornblende and Mg hastingsite with Mg no. ranging from 0.73 to 0.79. In rocks from the disseminated ore and the main Aguablanca intrusion, Mg hornblende, actinolitic hornblende, and minor pargasitic hornblende and Mg hastingsite predominate, with Mg no. varying from 0.70 to 0.86.

Phlogopite

In fragments, the Mg no. of phlogopite varies systematically with rock type: 0.85 to 0.89 in peridotite, 0.64 to 0.84 in anorthosite, 0.75 in pyroxenite, and 0.69 to 0.78 in gabbro. Phlogopite exhibits similar Mg no. values in both the gabbronorite matrix of semimassive and disseminated ore-bearing breccias, ranging from 0.69 to 0.84. In the gabbronorite and quartz-diorite rocks from the main Aguablanca intrusion, Mg no. values vary between 0.73 and 0.79, and 0.60 and 0.63, respectively.

Whole-Rock Geochemistry

Twenty-two rock samples, including mafic-ultramafic fragments, the gabbronorite matrix of the mineralized breccias, and rocks from the main Aguablanca intrusion were selected for whole-rock analyses. Major elements were determined by fusion-ICP and trace elements by ICP-MS at ACTLABS, Ontario, Canada. Representative analyses are summarized in Table 5.

TABLE 5. Representative Whole-Rock Major and Trace Element Compositions of Various Rock Types from the Aguablanca Ore Deposit

Location	Mafic-ultramafic fragments								Disseminated ore-bearing matrix			Main Aguablanca intrusion	
Rock type	Dunite	Werh.	Harz.	Gabbro[1]	Gabbro[2]	Anorth.	Gnorite	Hbl gabbro	Gnorite	Gnorite	Gdiorite	Gnorite	Q-diorite
Wt percent													
SiO_2	37.86	38.79	48.50	46.80	45.52	43.67	49.82	49.73	49.41	47.38	51.08	51.79	54.14
TiO_2	0.05	0..65	0.64	0.40	0.44	0.67	0.20	1.30	0.27	0.22	0.53	0.44	0.52
Al_2O_3	0.72	8.70	6.80	10.89	9.88	30.06	20.35	19.02	8.27	10.46	14.25	13.34	14.17
CaO	1.51	6.14	22.80	17.26	20.73	10.16	12.19	10.11	5.98	7.21	8.93	8.23	6.94
K_2O	0.19	0.31	0.04	0.37	0.46	2.10	0.39	0.86	0.40	0.44	1.23	0.57	1.26
MgO	39.89	25.45	14.68	12.54	10.06	2.98	8.26	6.97	17.09	14.68	10.90	13.66	9.64
MnO	0.25	0.36	0.21	0.32	0.21	0.05	0.13	0.10	0.22	0.16	0.13	0.15	0.16
Na_2O	0.08	0.49	0.23	0.82	0.36	1.92	1.86	3.80	1.05	1.32	2.69	1.86	2.91
P_2O_5	0.05	0.02	0.01	0.01	0.04	0.03	0.01	0.52	0.04	0.02	0.11	0.05	0.07
Fe_2O_3	15.21	11.14	4.94	7.61	8.89	5.07	5.67	6.16	14.58	14.98	6.73	8.27	7.72
L.O.I.	4.13	7.47	0.60	1.66	2.00	2.10	0.43	1.63	1.50	1.88	2.89	0.81	2.29
Total	99.94	98.87	99.45	98.68	98.59	98.81	99.31	100.20	98.81	98.75	99.47	99.17	99.82
Parts per million													
Cr	<20	112	137	405	982	209	733	222	1,220	803	556	881	559
Ni	1290	449	68	577	313	379	666	304	3,430	6,510	255	301	199
Cu	133	281	36	1510	1930	133	714	394	>10,000	8,950	180	66	10
Pb	5	14	<5	<5	27	<5	12	<5	20	36	<5	<5	<5
Rb	8	9	<2	14	17	97	13	26	19	19	49	15	38
Ba	34	229	23	181	239	1290	145	291	131	120	312	134	345
Th	0.1	1.2	1.1	0.6	1.1	0.8	0.1	1.6	2.2	0.7	3.5	1.3	4.2
U	<0.1	1	0.2	0.2	0.5	0.2	<0.1	0.6	0.6	0.2	0.6	0.4	0.9
Nb	<1	<1	3	2	2	2	<1	7	2	1	5	2	5
Ta	<0.1	0.1	0.7	<0.1	0.1	0.3	<0.1	0.5	0.1	<0.1	0.3	0.2	0.3
Sr	11	69	40	193	115	541	510	526	167	214	434	315	347
Y	1	7	17	19	10	2	6	37	8	8	15	10	19
Zr	8	320	178	56	61	43	14	89	28	19	73	27	72
La	1.1	4	11.7	5.8	4.6	12.7	4.6	27.9	5.7	5.2	16.8	7.3	27.1
Ce	2.5	9.5	30.4	16.3	11.8	18.3	8.9	61.7	11.3	10.6	33.5	16.2	52.9
Pr	0.28	1.27	3.75	2.49	1.52	1.72	0.99	8.04	1.32	1.2	3.83	1.89	5.45
Nd	1.2	5.9	14.5	13.1	7.3	6	4.3	36.5	5.5	5.5	15.3	8.5	21.7
Sm	0.3	1.6	3	3.9	2.1	0.9	1.2	8.8	1.3	1.4	3.2	2.3	4.4
Eu	0.07	0.41	0.59	0.97	0.52	0.78	0.61	1.91	0.4	0.45	0.92	0.73	1.28
Gd	0.2	1.7	3	4.2	2.1	0.6	1.3	8.9	1.4	1.4	3.2	2.2	4
Tb	<0.1	0.3	0.5	0.7	0.4	<0.1	0.2	1.4	0.2	0.2	0.5	0.4	0.6
Dy	0.2	1.5	2.8	3.7	2	0.4	1.3	7.4	1.4	1.4	2.7	2.1	3.7
Ho	<0.1	0.3	0.5	0.7	0.4	<0.1	0.3	1.4	0.3	0.3	0.5	0.4	0.8
Er	0.2	0.9	1.6	1.9	1.2	0.2	0.8	3.7	0.9	0.9	1.5	1.4	2.3
Tm	<0.05	0.14	0.24	0.28	0.17	<0.05	0.11	0.5	0.14	0.14	0.23	0.2	0.35
Yb	0.1	0.9	1.5	1.7	1.1	0.2	0.7	2.8	0.9	0.9	1.4	1.2	2.2
Lu	<0.04	0.15	0.24	0.26	0.15	<0.04	0.1	0.39	0.15	0.13	0.21	0.17	0.31
Hf	0.2	12.7	5.2	2.3	2.4	1.5	0.5	3.2	1	0.6	2.1	1	2.2
Cu/Zr	16.63	0.88	0.20	26.96	31.64	3.09	51.00	4.43	>357.14	471.05	2.47	2.44	0.14

Werh = hornblende-rich werhlite, Harz = hornblende-rich harzburgite, Anorth = anorthosite, Gnorite = gabbronorite, Hbl gabbro = hornblende gabbro, Gdiorite = gabbrodiorite

[1] Gabbro (cpx cumulus)

[2] Gabbro (cpx intercumulus)

Fragments

The fragments have bulk-rock compositions that reflect their primary mineralogy, with an overall increase in the SiO_2, Al_2O_3, TiO_2, alkali, Sr, and Ba concentrations with decreasing MgO. Primitive mantle-normalized trace incompatible element profiles show significant enrichments in all the large ion lithophile elements (LILE), Rb, Ba, Th, U, and the LREE, relative to the high field strength elements (HFSE) Ta, Nb, Ti, Zr, Hf, and HREE, strong positive Pb anomalies, and some positive Sr anomalies related to the amount of plagioclase (Fig. 7A). Gabbronorite is anomalously enriched in Ti owing to the presence of ilmenite. The larger variations in K and Ba compared to most of the elements can be attributed to mobility during alteration. The fragments have variable REE contents, reflecting different abundances of intercumulus material and amphibole, but they are uniformly enriched in LREE relative to HREE (Fig. 7A), with $(La/Lu)_N$ ratios from 2.7 to 7.7 and much higher (51.2) in the anorthosite. Gabbronorite and anorthosite exhibit slightly positive Eu anomalies related to plagioclase fractionation.

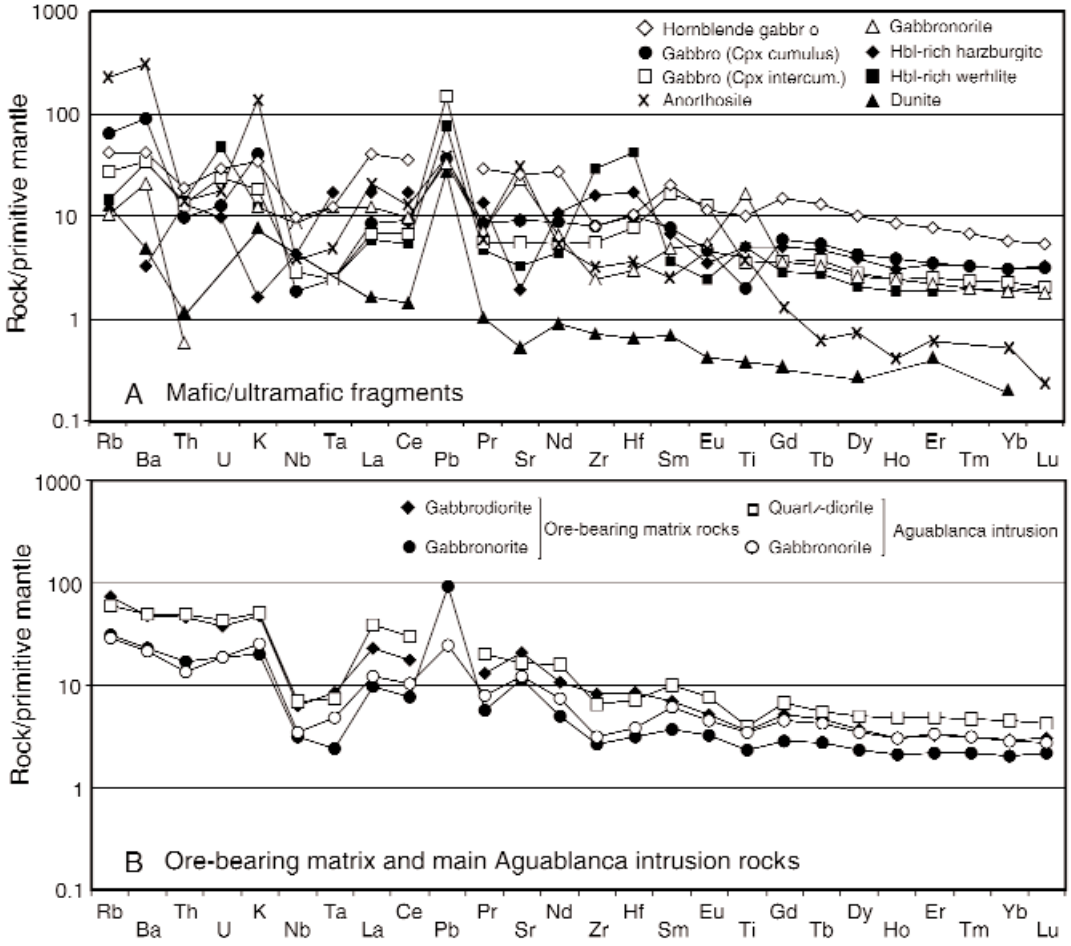

FIG. 7. Primitive mantle-normalized, trace incompatible element patterns for rocks from the (A) mafic-ultramafic fragments and (B) rocks from the main Aguablanca intrusion and the ore-bearing matrix rocks in the breccia. Patterns were drawn from the average, whole-rock values for each different lithology. Primitive mantle values are from Sun and McDonough (1989).

Gabbronorite matrix of the ore-bearing breccias and rocks from the main Aguablanca intrusion

In terms of major elements, gabbronorite in the mineralized matrix and the main Aguablanca intrusion have very similar compositions (Table 5), and quartz-diorite from the main Aguablanca intrusion has more evolved compositions (Table 5). Primitive mantle-normalized trace incompatible element patterns of the gabbronorite matrix in the disseminated ore-bearing breccias and gabbrodiorite are comparable to those of the main Aguablanca intrusion (Fig. 7B). They are characterized by strong enrichments in LILE relative to HFSE, and by strong positive Pb and lesser Sr anomalies. $(La/Lu)_N$ ratios average 4.51, 7.45, and 9.37 for gabbronorite, gabbrodiorite, and quartz-diorite, respectively. Trace incompatible elements and REE abundances are significantly higher in gabbrodiorite and quartz-diorite in the main intrusion than in the gabbronorite matrix of the breccias.

Discussion

Origin of the mafic-ultramafic fragments

Several features of the breccias suggest that the fragments were derived from previously crystallized rocks that were brecciated and emplaced as solid (or semisolid) clasts. These include subangular to rounded shapes with straight boundaries, sharp contacts with the matrix, tabular crystals of plagioclase in the matrix outlining the fragments (suggesting the flow of a crystal-charged magma adapting to the fragments), and nucleation of matrix crystals on the surfaces of the fragments, indicating heterogeneous nucleation (Chernov, 1984). The fine grain size of the cumulus crystals in some fragments (Fig. 5F) suggests that they represent primary crystals for which recrystallization to a coarser grain size was inhibited. The fine grain size of the fragments indicates that these rocks probably were at their initial stages of crystallization as partially consolidated material when they were brecciated. The transport of the fragments upward within the matrix melt likely took place under conditions of rapid cooling, preventing the textural coarsening (e.g., by Ostwald ripening: Park and Hanson, 1999). The subangular shapes and the lack of embayed or penetrated boundaries in the fragments rule out assimilation processes by the enclosing melt. The emplacement and cooling of the sulfide-rich and fragment-charged magma were rapid enough to inhibit assimilation. Heating effects during transport of the fragments by the host magma are apparent in the equigranular and polygonal textures in some

fragments of dunite, gabbro, or orthopyroxenite (Fig. 5C, E), which likely resulted from subsolidus recrystallization processes (e.g., Frey and Prinz, 1978; Scribbins et al., 1984).

Four possible sources may be considered for the fragments at Aguablanca: (1) the mantle, (2) outcrop of pre-Aguablanca mafic-ultramafic bodies, (3) the main Aguablanca intrusion, or (4) a hidden differentiated (layered?) mafic-ultramafic sequence situated beneath the Aguablanca intrusion.

The fragments have a number of characteristics similar to those described by Scribbins et al. (1984), for similar fragments in the sublayer of the Sudbury Igneous Complex, that rule out their origin as mantle-derived nodules. Despite subsolidus recrystallization processes, the fragments commonly preserve original cumulate textures, whereas mantle nodules typically exhibit features of plastic flow and solid-state deformation with metamorphic textures. Dunite, harzburgite, wehrlite, pyroxenite, and plagioclase-bearing rocks are typical of differentiated complexes, whereas mantle nodules are mainly lherzolite and eclogite. In mantle nodules, the dominant oxide mineral is commonly chrome spinel, not a Cr-free spinel as in the fragments. Finally, the extensive presence of abundant plagioclase, implying a depth of 25 to 30 km or less for final equilibration (Green and Hibberson, 1970), is indicative of a crustal origin.

An association of the fragments with outcrop of pre-Aguablanca intrusive bodies can also be excluded, as the nearby calc-alkaline Santa Olalla (Casquet, 1980) and alkaline Garrote and Castillo granitic bodies (Eguiluz et al., 1999) have petrological and geochemical features that are very different from the fragments.

The main unmineralized Aguablanca intrusion also cannot be considered the source of the fragments, as some rock types of the fragments (i.e., pyroxenites, anorthosites, and peridotites) do not occur elsewhere in the intrusion. The gabbronorite from the main Aguablanca intrusion is also texturally different from the gabbronoritic fragments, the latter being much finer, with different mineral habits (Fig. 5F) and more abundant ilmenite than in the main Aguablanca intrusion. However, the intimate relationship between the fragments and the gabbronorite matrix in the ore breccia, and the petrological and geochemical similarities between the matrix of the fragments and the rocks of the main Aguablanca intrusion suggest a genetic link. The trace element normalized-patterns of the fragments show some similarities to those of the gabbronorite matrix of the breccia and to the rocks of the Aguablanca intrusion (Fig. 7), including an overall enrichment in LILE and LREE relative to HFSE and HREE, and pronounced positive Pb and negative Nb and Ta anomalies. This suggests that the different parent melts were likely cogenetic and derived from the same magmatic source.

A mafic-ultramafic differentiated complex seems the most plausible source of the fragments, as previously suggested by Tornos et al. (2001), in which the fragments and source rocks represent different stages of cumulate formation. Several features of the fragments support this interpretation: (1) they exhibit cumulate textures, with commonly poikilitic minerals (Fig. 5C, D); (2) they include a wide variety of rock types, from ultramafic (dunite, harzburgite, werhlite, and pyroxenite) to mafic (gabbronorite, gabbro, hornblende gabbro, and anorthosite), possibly reflecting fractional crystallization in the source; (3) composite fragments consist of clinopyroxenite-anorthosite, with well-marked boundaries, possibly preserving contact relationships between preexisting layers in the source complex; (4) the grain size and cryptic layering of the gabbro fragments is typical of magmas that have undergone differentiation (Fig. 6); and (5) Fe enrichment trends in the magmatic ferromagnesian minerals (Fig. 8) likely represent progressive differentiation of the melts.

Relationship between the matrix of the ore-bearing breccias and the main Aguablanca intrusion

There are a number of important similarities between the rocks of the main Aguablanca intrusion and the gabbronorite matrix of the ore breccias. In both gabbronorites, pyroxene crystallized as a cumulus phase, amphibole and phlogopite crystallized as intercumulus phases, and plagioclase occurs in a wide range of modal abundances both as a cumulus and intercumulus phase (Figs. 2A, 5B). The geochemistry of the bulk rock and the compositions of the primary silicate phases are also similar (Tables 2, 5). Concentrations and primitive mantle-normalized patterns of the trace incompatible elements are identical (Fig. 7B). Gabbronorite, gabbrodiorite, and quartz-diorite from the matrix of the ore breccias and in the main Aguablanca intrusion show well-defined differentiation trends as indicated by the progressive increase in the trace incompatible element abundances from gabbronorite to gabbrodiorite and quartz-diorite (Fig. 7B) and the more evolved mineral compositions in the quartz-diorite in comparison to the gabbronorite (Table 2). The main Aguablanca intrusion contains minor mafic-ultramafic fragments that are similar to those of the ore-bearing breccia. These features suggest that the rocks of the main Aguablanca intrusion and the matrix of the ore-bearing breccias belong to the same magmatic suite, with the main Aguablanca intrusion representing a sulfide-free equivalent of the fragment- and ore-bearing rocks. In this model, the barren gabbrodiorites of the Aguablanca intrusion would represent early injections of

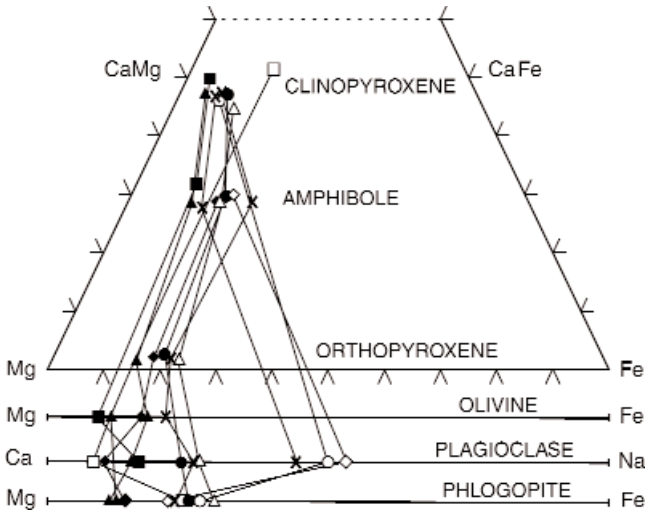

FIG. 8. Compositional variation in the magmatic silicate minerals from the fragments. See Figures 6 and 7 for symbols. The average compositions of the relevant minerals are shown for each rock type. Tie lines indicate coexisting phases.

differentiated melts from the top of the magma chamber, whereas the ore breccia would represent the latest injection which contained sulfide melt, the fragments, and the remaining differentiated, gabbronoritic melt.

Segregation of the sulfide liquid

The mineralogic and textural characteristics of the sulfides indicate that the mineralization is the result of the magmatic crystallization and subsolidus reequilibration of a sulfide melt segregated from a mafic-ultramafic magma (Ortega et al., 2004; Piña et al., 2005). Geochemical data suggest that sulfide liquid unmixed from the silicate melt before the fractionation of some peridotite cumulates in the differentiated complex. Mg-rich olivine in the werhlite and dunite fragments has very low Ni contents (below 0.07 wt %), pointing to a Ni-depleted parental melt (Duke and Naldrett, 1978; Campbell and Naldrett, 1979; Thompson and Naldrett, 1984). Cu/Y ratios are positively correlated with the Cu/Zr ratios (Fig. 9) and some peridotite fragments (hornblende-rich werhlite and hornblende-rich harzburgite) have Cu/Zr ratios below 1. Lightfoot et al. (1994), Li et al. (2000), Kerr et al. (2001), and Song et al. (2003) have shown that Cu/Zr ratios below 1 are indicative of depletion in Cu by the segregation of sulfide liquid. The trace element data, therefore, support the interpretation of sulfide segregation before and/or during the fractionation of peridotite cumulates in the differentiated complex.

The presence of disseminations of sulfides in some fragments (e.g., hornblende-rich harzburgite contains 5 modal % sulfide) indicates trapping of sulfide liquid during silicate crystallization, although the possibility that these sulfides could also represent some infiltration from the sulfide-rich matrix cannot be ruled out. The abundance of the sulfides within the matrix of the breccia and the very low sulfide content of the fragments indicate that the sulfide liquid was efficiently removed from the cumulate pile. The sulfide melt likely concentrated toward the floor of the magmatic chamber, leaving the uppermost differentiated silicate melt almost completely free of sulfide melt. Upward injection of a batch of silicate magma containing unsettled sulfide liquid also is indicated by the presence of sulfide droplets interstitial to the silicates in the disseminated ore (i.e., fig. 6A of Ortega et al., 2004).

The sulfur isotope composition of Aguablanca sulfides is close to 7.4 per mil (Casquet et al., 1999), indicating crustal contamination. Casquet et al. (2001) and Tornos et al. (2001) argued that sulfur saturation of the parental melt was attained as a consequence of the local assimilation of upper Precambrian pyrite-bearing black slates (Serie Negra) which can contain up to 3,000 ppm of sulfur (R. Piña, unpub data). The lead isotope signature of the ore ($^{206}Pb/^{204}Pb$ = 18.27–18.43; $^{207}Pb/^{204}Pb$ = 15.61–15.65) is also similar to that of the metasedimentary country rocks (Tornos and Chiaradia, 2004). The systematic enrichment of the fragments in Pb, LILE, and LREE relative to HFSE and HREE (Fig. 7A) is also evidence of crustal contamination (e.g., Zhou et al., 2004).

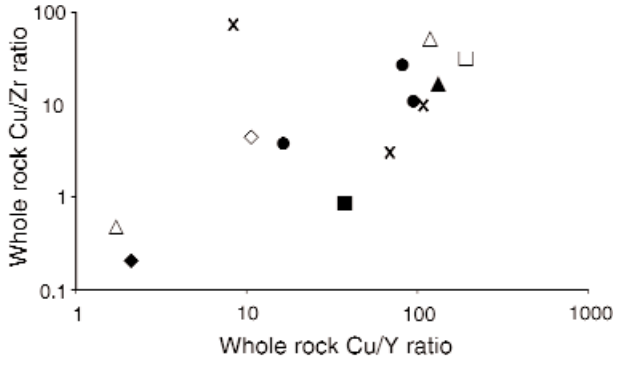

FIG. 9. Plot of Cu/Y versus Cu/Zr for the mafic-ultramafic fragments. See Figures 6 and 7 for symbols.

Genesis and geodynamic context of the Aguablanca ore deposit

Unlike most of the plutonic Ni-Cu sulfide deposits, which occur at the base or related to specific levels of mafic igneous intrusions, Aguablanca is a subvertical magmatic breccia. This form requires a much more energetic setting than that of the Ni-Cu deposits in layered mafic complexes and indicates that rupture of the inferred ultramafic complex beneath Aguablanca was the key process in the emplacement of the deposit. The sulfide protore was likely generated in an environment similar to that of most plutonic Ni-Cu deposits, but multiple magma injections likely occurred in an open system, as indicated by the decoupling between mineral chemistry and modal compositions of the fragments (e.g., dunite having more differentiated olivine compositions, $Fo_{88–83}$, than those of werhlite, $Fo_{91–90}$). As already noted by Tornos et al. (2001), the brecciation of the cumulate sequence took place at temperatures well above the mss solidus (approx 950ºC) but below that of olivine and pyroxene. This would give rise to a system where the sulfide liquid enveloped partially or totally consolidated cumulates. With the drop in temperature because of the emplacement at shallower crustal levels, the sulfide liquid crystallized.

Several mechanisms have been proposed to explain the rupture of the inferred mafic-ultramafic complex at depth, such as the opening of a zone of weakness within the differentiating magma chamber, tectonic squeezing or seismic plumping (Tornos et al., 2001), or the development of dilational structures related to major faults (Casquet et al., 2001). The mineralogy and mineral chemistry of silicates in the gabbronorite matrix of the ore-bearing breccia indicate that they crystallized from less fractionated melts than many fragments. In particular, the gabbronorite matrix has more primitive modal compositions than some fragments (e.g., gabbro, hornblende gabbro). Clinopyroxene from the matrix has higher Cr contents than clinopyroxene in the fragments (many with <0.05 wt % and below detection limit of microprobe; Table 3), suggesting that the magma forming these rocks was more primitive than that of the fragments (cf. Barnes and Hoatson, 1994). Although there is no evidence for a volatile-rich magma in the system, the brecciation of the cumulates and the upward displacement of the sulfide liquids and the fragments might have been caused by the injection of a pulse of more fractionated magma into the magma chamber. This new magma picked up the early segregated sulfide melt and disrupted the overlying cumulates, rapidly transporting them to their current position as fragments and concentrating the sulfides in the form of a

subvertical breccia. The high density of the sulfide-charged batch of magma helped to entrain fragments more easily; hence, the close spatial relationship of the fragments to the sulfides. The barren Aguablanca intrusion and the disseminated ore could be products of earlier injections from the main differentiating complex.

The Aguablanca ore deposit is temporally related to the development of an Andean-type continental magmatic arc associated with the subduction of the South Portuguese zone beneath the Ossa-Morena zone during the Hercynian orogeny (Eguiluz et al., 2000). The rocks of the main Aguablanca intrusion display the characteristic features of subduction zone magmas enriched by subduction-related components (Fig. 7A, B): strong enrichment in LILE and Pb, slight enrichment in LREE with respect to HREE, and depletion of Nb and Ta (Perfit et al., 1980). The geodynamic context of the Aguablanca ore deposit, therefore, contrasts with most other Ni-Cu deposits that are closely related to rift settings (Lesher, 1997) and only rarely occur in compressive orogenic environments (e.g., the Moxie pluton: Thompson and Naldrett, 1984; the Caledonian intrusions of northeast Scotland: Fletcher, 1987; the Rana intrusion: Boyd and Mathisen, 1979). Recent geophysical studies of the southwest Iberian Peninsula (seismic reflection profile, IBERSEIS: Simancas et al., 2003) have revealed the presence of a thick, sill-like structure represented by a long high-amplitude reflective band in a mid-crustal decollement. This band has been interpreted as a huge, structurally layered mafic-ultramafic complex related to a mantle plume, which was active during the period 355 to 335 Ma, and emplaced during a short extensional stage during the development of the Hercynian magmatic arc. This mantle-derived mafic-ultramafic magmatism developed beneath the Ossa-Morena zone and may have been the source of the parental magmas of Aguablanca. If true, the whole of southwest Iberia could be a region with a high potential for other similar Ni-Cu-(PGE) deposits.

Acknowledgments

This work was made possible by Rio Narcea Recursos, which provided access to drill core and geologic information. Appreciation is expressed to the technical staff of Rio Narcea Recursos at the Aguablanca mine, notably to the geologists C. Maldonado, E. J. Martínez, and C. Fernández, for their assistance during our studies of the deposit. Our work has greatly benefited from the geologic advice of and discussions with R. Capote, C. Quesada, and I. Romeo. We would like to thank J. González del Tánago and A. Larios from the Centro de Microscopía Electrónica "Luis Bru" in the University Complutense of Madrid and of the Institute of Electron Optics in the University of Oulu, Finland, for their assistance with the electron microprobe in the chemical analyses of the minerals. We thank two reviewers, Michael Lesher and Jean Bedard, for their constructive reviews, and Mark Hannington for his editorial input which has helped to improve the manuscript. This research was supported by the Spanish Ministry of Education and Science, Project BTE2003-03599.

REFERENCES

Alapieti, T., and Lahtinen, J., 2002, Platinum-group element mineralization in layered intrusions of northern Finland and the Kola Peninsula, Russia, *in* Cabri, L.J., ed., The geology, geochemistry, mineralogy and mineral beneficiation of platinum-group elements: Canadian Institute of Mining, Metallurgy and Petroleum Special Volume 54, p. 507–546.

Barnes, S.J., and Hoatson, D.M., 1994, The Munni Munni Complex, Western Australia: stratigraphy, structure and petrogenesis: Journal of Petrology, v. 35, no. 3, p. 715–751.

Barnes, S.J., Melezhik, V.A., and Sokolov, S.V., 2001, The composition and mode of formation of the Pechenga nickel deposits: Canadian Mineralogist, v. 39, p. 447–471.

Berg, J.H., 1980, Snowflake troctolite in the Hettasch intrusion, Labrador: Evidence from magma-mixing and supercooling in a plutonic environment: Contributions to Mineralogy and Petrology, v. 72, p. 339–351.

Boyd, R., and Mathisen, C.O., 1979, The nickel mineralization of Råna mafic intrusion, Nordland, Norway: Canadian Mineralogist, v. 17, p. 287–298

Campbell, I.H., and Naldrett, A.J., 1979, The influence of silicate:sulfide ratios on the geochemistry of magmatic sulfides: Economic Geology, v. 74, p. 1503–1505.

Casquet, C., 1980, Fenomenos de endomorfismo, metamorfismo y metasomatismo de contacto en los mármoles de Rivera de Cala (Sierra Morena): Unpublished M.Sc. thesis, Madrid, Spain, University Complutense, p. 295.

Casquet, C., Eguiluz, L., Galindo, C., Tornos, F., and Velasco, F., 1999, The Aguablanca Cu-Ni-(PGE) intraplutonic ore deposit (Extremadura, Spain). Isotope (Sr, Nd, S) constraints on the source and evolution of magmas and sulphides: Geogaceta, v. 24, p. 71–72.

Casquet, C., Galindo, C., Tornos, F., Velasco, F., and Canales, A., 2001, The Aguablanca Ni-Cu-(PGE) intraplutonic ore deposit (Extremadura, Spain), a case of synorogenic orthomagmatic mineralization: Age and isotope composition of magmas (Sr, Nd) and (S): Ore Geology Reviews, v. 18, p. 237–250.

Chernov, A.A., 1984, Modern crystallography III: Crystal growth: Berlin, Springer-Verlag, 517 p.

Duke, J.M., and Naldrett, A.J., 1978, A numerical model of the fractionation of olivine and molten sulfide from komatiite magma: Earth and Planetary Science Letters, v. 39, p. 255–266.

Eguiluz, L., Apraiz, A., and Abalos, B., 1999, Structure of the Castillo Granite, southwest Spain; Variscan deformation of a late Cadomian pluton: Tectonics, v. 18, p. 1041–1063.

Eguiluz, L., Gil Ibarguchi, J.I., Abalos, B., and Apraiz, A., 2000, Superposed Variscan and Cadomian orogenic cycles in the Ossa-Morena zone and related areas of the Iberian Massif: Geological Society of the American Bulletin, v. 112, p. 1398–1413.

Evans-Lamswood, D.M., Butt, D.P., Jackson, R.S., Lee, D.V., Muggridge, M.G., Wheeler, R.I., and Wilton, D.H.C., 2000, Physical controls associated with the distribution of sulfides in the Voisey's Bay Ni-Cu-Co deposit, Labrador: Economic Geology, v. 95, p. 749–769.

Féménias, O., Coussaert, N., Bingen, B., Whitehouse, M., Mercier, J.C.C., and Demaiffe, D., 2003, A Permian underplating event in late- to post-orogenic tectonic setting: Evidence from the mafic-ultramafic layered xenoliths from Beaunit (French Massif Central): Chemical Geology, v. 199, p. 293–315.

Fletcher, T.A., 1987, Nickel-copper and precious metal mineralization in the Caledonian mafic and ultramafic intrusions of north-east Scotland [abs], *in* Prichard, H.M., Potts, P.J., Bowles, J.F.W. and Cribb, S.J., eds., Geoplatinum 87: Elsevier, p. 163.

Frey, F.A., and Prinz, M., 1978, Ultramafic inclusions from San Carlos, Arizona: Petrologic and geochemical data bearing on their petrogenesis: Earth and Planetary Science Letters, v. 38, p. 129–176.

Frietsch, R., Papunen, H., and Vokes, F.M., 1979, The ore deposits in Finland, Norway and Sweden: A review: Economic Geology, v. 74, p. 975–1001.

Garuti, G., Fiandri, P., and Rossi, A., 1986, Sulphide composition and phase relations in the Fe-Ni-Cu ore deposits of the Ivrea-Verbano basic complex (western Alps, Italy): Mineralium Deposita, v. 21, p. 22–34.

Green, D.H., and Hibberson, W., 1970, The instability of plagioclase in peridotite at high pressure: Lithos, v. 3 p. 209–221.

Kerr, A., MacDonald, H.E., and Naldrett, A.J., 2001, Geochemistry of the Pants Lake intrusion, Labrador: Implications for future mineral exploration: Government of Newfoundland and Labrador, Department of Mines and Energy, Geology Survey, Report 2001-1, p. 191–228.

Leake, T.N., 1978, Nomenclature of amphiboles: American Mineralogist, v. 63, p. 1023–1053.

Lesher, C.M., 1997, Temporal evolution of magmatic Fe-Ni-Cu-(PGE) sulfide deposits [abs]: Geological Society of America Abstract with Programs, v. 29, no. 6, p. 15.

Li, C., Lightfoot, P.C., Amelin, Y., and Naldrett, A.J., 2000, Contrasting petrological and geochemical relationships in the Voisey's Bay and Mushuau intrusions Labrador, Canada: Implications for ore genesis: Economic Geology, v. 95, p. 771–800.

Lightfoot, P.C., Naldrett, A.J., Gorbachev, N.S., Fedorenko, V.A., Hawkesworth, C.J., and Doherty, W., 1994, Chemostratigraphy of Siberian flood basalts lava, Noril'sk district, Russia: Implications and source of flood basalt magmas and their associated Ni-Cu mineralisation, *in* Lightfoot, P.C., Naldrett, A.C., eds., Proceedings of the Sudbury-Noril'sk Symposium: Ontario Geological Survey Special Publication, v. 5, p. 283–312.

Lunar, R., García-Palomero, F., Ortega, L., Sierra, J., Moreno, T., and Prichard, H., 1997, Ni-Cu-(PGM) mineralization associated with mafic and ultramafic rocks: The recently discovered Aguablanca ore deposit, SW Spain, *in* Papunen, H., ed., Mineral deposits: Research and exploration: Where do they meet?: Rotterdam, The Netherlands, Balkema, p. 463–466.

Mathison, C.I., 1987, Pyroxene oikocrysts in troctolitic cumulates-evidence for supercooled crystallisation and postcumulus modification: Contributions to Mineralogy and Petrology, v. 97, p. 228–236.

Ortega L., Prichard, H., Lunar, R., García Palomero, F., Moreno, T., and Fisher, P., 2000, The Aguablanca discovery: Mining Magazine, v. 2, p. 78–80.

Ortega, L., Lunar, R., García Palomero, F., Moreno, T., Martín Estévez, J.R., Prichard, H.M., and Fisher, P.C., 2004, The Aguablanca Ni-Cu-PGE deposit, southwestern Iberia: Magmatic ore-forming processes and retrograde evolution: Canadian Mineralogist, v. 42, p. 325–350.

Park, Y., and Hanson, B., 1999, Experimental investigation of Oswald ripening rates of forsterite in the haplobasaltic system: Journal of Volcanology and Geothermal Research, v. 90, p. 103–113.

Perfit, M.R., Gust, D.A., Bence, A.E., Arculus, R.J., and Taylor, S.R., 1980, Chemical characteristics of island-arc basalts: Implications for mantle sources: Chemical Geology, v. 30, p. 227–256.

Piña, R., Gervilla, F., Ortega, L., and Lunar, R., 2005, Geochemistry and mineralogy of platinum-group elements in the Aguablanca Ni-Cu deposits (SW Spain), *in* Törmänen, T.O., and Alapieti, T.T., eds., 10th International Platinum Symposium: Oulu, Finland, Extended Abstracts, p. 215–218.

Quesada, C., 1991, Geological constraints on the Paleozoic tectonic evolution of the tectonostratigraphic terranes in the Iberian Massif: Tectonophysics, v. 185, p. 225–245.

Romeo, I., Lunar, R., Capote, R., Quesada, C., Dunning, G.R., Piña, R., and Ortega, L., 2004, Edades de cristalización U-Pb en circones del complejo ígneo de Santa Olalla de Cala: Implicaciones en la edad del yacimiento de Ni-Cu-EGP de Aguablanca (Badajoz): MACLA, v. 2, p. 29–30.

Sánchez Carretero, R., Eguiluz, L., Pascual, E., and Carracedo, M., 1990, Igneous rocks of the Ossa-Morena zone, *in* Dallmeyer, R.D., and Martínez García, E., eds., Pre-Mesozoic geology of Iberia: Heidelberg, Springer-Verlag, p. 292–313.

Sánchez-García, T., Bellido, F., and Quesada, C., 2003, Geodynamic setting and geochemical signatures of Cambrian-Ordovician rift-related igneous rocks (Ossa-Morena zone, SW Iberia): Tectonophysics, v. 265, p. 233–255.

Scribbins, B.T., Donald, R.R., and Naldrett, A.J., 1984, Mafic and ultramafic inclusions in the sublayer of the Sudbury igneous complex: Canadian Mineralogist, v. 22, p. 67–75.

Simancas, J.F., Carbonell, R., González Lodeiro, F., Pérez Estaún, A., Juhlin, C., et al., 2003, Crustal structure of the transpressional Variscan orogen of SW Iberia: SW Iberia deep seismic reflection profile (IBERSEIS): Tectonics, v. 22, 1062, dpi: 10.1029/2002TC001479.

Snoke, A.W., Quick, J.E., and Bowman, H.R., 1981, Bear Mountain igneous complex, Klamath Mountains, California: An ultrabasic to silicic calc-alkaline suite: Journal of Petrology, v. 22, p. 501–552.

Song, X.Y, Zhou, M.F., Cao, Z.M., Sun, M., and Wang, Y.L., 2003, Ni-Cu-(PGE) magmatic sulfide deposits in the Yangliuping area, Permian Emeishan igneous province, SW China: Mineralium Deposita, v. 38, p. 831–843.

Sun, S.S., and McDonough, W.F., 1989, Chemical and isotopic systematics of oceanic basalts: implication for mantle composition and processes, *in* Saunders, A.D., and Norry, M.J., eds., Magmatism in the ocean basins: Geological Society London Special Publication, v. 42, p. 313–345.

Thompson, J.F.H., and Naldrett, A.J., 1984, Sulfide-silicate reactions as a guide to Ni-Cu-Co mineralization in central Maine, *in* Buchanan D.L., and Jones, M.J., eds., Sulfide deposits in mafic and ultramafic rocks: London, Institution of Mining and Metallurgy, Special Publication, p. 103–113.

Tornos, F., and Chiaradia, M., 2004, Plumbotectonic evolution of the Ossa-Morena zone, Iberian Peninsula: Tracing the influence of mantle-crust interaction in ore-forming processes: Economic Geology, v. 99, p. 965–985.

Tornos, F., Casquet, C., Galindo, C., Velasco, F., and Canales, A., 2001, A new style of Ni-Cu mineralization related to magmatic breccia pipes in a transpressional magmatic arc, Aguablanca, Spain: Mineralium Deposita, v. 36, p. 700–706.

Tornos, F., Iriondo, A., Casquet, C., and Galindo, C., 2004, Geocronología Ar-Ar de flogopitas del stock de Aguablanca (Badajoz): Implicaciones sobre la edad del plutón y de la mineralización de Ni-(Cu) asociada: Geotemas, v. 6, p. 189–192.

Zhou, M.F., Lesher, C.M., Yang, Z., Li, J., and Sun, M., 2004, Geochemistry and petrogenesis of 270 Ma Ni-Cu-(PGE) sulfide-bearing mafic intrusions in the Huangshan district, eastern Xinjiang, northwest China: Implications for the tectonic evolution of the central Asian orogenic belt: Chemical Geology, v. 209, p. 233–257.